AN ABSTRACT OF THE THESIS OF

Ayako Nakagawa for the degree of Master of Science
in Chemical Engineering presented on July 22, 2008.
Title : Catalytic Chemical Vapor Deposition Synthesis of Carbon Nanotubes from Methane on SiO Supported Fe and Fe−Ni Catalysts

Abstract approved:_____
Shoichi Kimura

Influences of operating conditions on the production of carbon nanotubes (CNTs) were studied using Fe and Fe-Ni bimetallic catalysts supported on silicon monoxide (SiO). The catalysts were prepared in three steps: (1) impregnation of SiO powders with ferric nitride or combinations of ferric and nickel nitrides, (2) oxidation of nitrides in an air stream, and (3) grinding the powders obtained. CNTs were successfully synthesized by catalytic CVD using NH_3/CH_4 mixtures in a horizontal tubular flow reactor. The following process parameters were varied to investigate their effects on the growth rates of CNTs. The morphologies of catalysts and product CNTs were observed by scanning electron microscope (SEM).

- The particle size of SiO,
- metal composition,
- metal loading,
- temperature for catalyst oxidation,
- extent of grinding of catalysts,
- NH_3 pretreatment time,

- reaction temperature for CNT growth,
- reaction time, and
- NH_3/CH_4 feed ratio.

Two different average sizes of SiO particles, 8 μm and 44 μm, were compared based on the growth of CNTs in 5 min. Catalysts supported on 44 μm average sized SiO particles demonstrated higher yields when they were not pretreated in an NH_3 stream. When 1 wt% Fe was loaded, aligned CNTs were formed, and a highest growth rate per unit mass of catalyst was observed. The range of oxidation temperature to achieve highest catalyst activities depended on metals and metal contents: 600 - 750°C for 1 wt% Fe, 450 - 600°C for 3 wt% Fe, and 750 - 900°C for Fe-Ni. Grinding catalysts for at least 3 minutes increased the growth rate of CNTs by approximately 40 percent. The growth of CNTs was enhanced when no NH_3 pretreatment of catalysts was carried out, regardless of metals and metal contents. However, CNTs did not grow appreciably from methane without ammonia. An NH_3/CH_4 feed ratio of 0.15 - 0.25 was observed to yield highest growth rates. The reaction temperature to achieve highest CNT growth rates was found to be in the range between 990 and 1000 °C. The growth of CNTs was not linear but decreased with reaction time.

Catalytic Chemical Vapor Deposition Synthesis of Carbon Nanotubes from Methane on SiO Supported Fe and Fe−Ni Catalysts

by
Ayako Nakagawa

A THESIS

submitted to

Oregon State University

in partial fulfillment of
the requirements for the
degree of

Master of Science

Presented July 22, 2008
Commencement June 2009

Master of Science thesis of Ayako Nakagawa
presented on July 22, 2008.

APROVED:

_____

Major Professor, representing Chemical Engineering

_____

Head of the School of Chemical, Biological, and Environmental Engineering

_____

Dean of the Graduate School

I understand that my thesis will become part of the permanent collection of Oregon State University libraries. My signature below authorizes release of my thesis to any reader upon request.

_____

Ayako Nakagawa, Author

ACKNOWLEDGEMENTS

I would like to express sincere appreciation to Dr. Kimura, my major professor, who has been instrumental in accomplishing this project. Without his assistance and teaching, this project would not have been completed. I sincerely thank him for his patience, technical insights, and warm consideration. I could learn many things throughout the entire work from him.

I would also like to thank Dr. Yokochi for spending his valuable time and lending his expertise in using a special SEM unit in his lab. I would like to thank Dr. Lerner and Dr. Koch who have provided me with useful information and knowledge for my research work in the field of chemistry. I would like to express my sincere appreciation to each of the committee members for having spared precious time for my defense.

I would like to thank my mentors and colleagues in Japan, who have always given valuable advice and encouragement.

I would like to thank my parents, brother, and sister for their continuous support and encouragement which have been big help for my stay.

Finally, I would like to express my sincere gratitude to my husband for his thoughtfulness, support, and encouragement in all aspects. I would like to give him the same kind of motivation and support forever.

TABLE OF CONTENTS

TABLE OF CONTENTS (Continued)

TABLE OF CONTENTS (Continued)

TABLE OF CONTENTS (Continued)

LIST OF FIGURES

LIST OF FIGURES (Continued)

LIST OF FIGURES (Continued)

LIST OF FIGURES (Continued)

LIST OF APPENDIX FIGURES

LIST OF APPENDIX FIGURES (Continued)

LIST OF TABLES

1 INTRODUCTION

Following the discovery of fullerenes, the soccer-ball shaped C_{60} clusters, by Kroto, et. al. in 1985 [1], carbon nanotubes (CNTs) were discovered by Iijima in 1991 [2]. Carbon nanotubes have very simple chemical composition and atomic bonding configurations, but they represent outstanding chemical and physical properties associated with their diverse structures. Based on their electronic, mechanical, optical, and chemical characteristics, a variety of potential applications have been suggested, such as a composite for reinforcements, a field emitter for flat panel displays, and chemical sensors. The large-scale production of purified CNTs for practical use has been eagerly studied.

For the synthesis of CNTs, several methods have been already developed, including arc-discharge, laser vaporization of graphite targets, electrolysis of carbon electrodes in molten halide salts, and various types of chemical vapor deposition (CVD). The first two techniques come from the same principle basically, in which the plasma produced by the evaporation of high-purity graphite electrodes condenses and forms single-walled carbon nanotubes (SWNTs) or multi-walled carbon nanotubes (MWNTs). Electrolysis is performed using a graphite anode and cathode in a liquid phase, and SWNTs and MWNTs can be made by the erosion of the cathode. In the CVD, different energy sources and support materials are used depending on the techniques. The growth of CNTs is mainly achieved by the thermal decomposition of hydrocarbon vapor, such as ethylene (C_2H_4) and methane (CH_4), over transition metal catalysts, such as Fe, Ni, Co, and Mo. Silica (SiO_2), alumina (Al_2O_3), or magnesium oxide (MgO) are mainly used as a support material.

Each of the above mentioned techniques has some advantages and disadvantages in the synthesis of CNTs. For instance, only the electrical arc discharge and laser vaporization can produce SWNTs with high crystallinity, but their production rates seem to be smaller compared to the catalytic CVD (CCVD) method [3, 4]. Electrolysis may be the least expensive way for synthesizing MWNTs due to its simple apparatus, raw energy consumption, such as low reaction temperature, and inexpensive raw materials [5, 6], but some issues, including the endurance of a cathode and low yields of products, have to be resolved. In the CCVD, the achievement in large-scale production has already been reported using a fluidized-bed reactor capable of producing 50 kg of carbon materials a day with a yield of 70 - 80% CNTs or 15 kg/h with a purity of 99.9% [7, 8]. Therefore, the CCVD seems to be most promising for mass production of high quality CNTs at low cost, and we have focused on this technique.

For the large-scale production in the CCVD, there are still some difficulties, including expensive raw materials, systematic purification of CNTs, namely removal of supporting substrates, and construction of continuous processes. A major cost increase is usually attributed to the purification that requires acid or alkali treatment followed by washing with de-ionized water for pH adjustment. To resolve these difficulties, a combination of CH_4 and silicon monoxide (SiO) has been developed by Kimura and Williamson in 2006 as one of least expensive carbon sources and support materials, respectively [9]. CH_4 is the major component (about 87%) of natural gases and very abundant. Silicon monoxide has positive possibilities for its elimination from

CNTs when it is heated at high enough temperature. Since SiO sublimates to SiO vapor at temperature above approximately 930°C and condenses as SiO_2 and Si mixtures at low temperature [10-16], it may be collected under vacuum conditions for recycle use. This recycle use of SiO will be effective for a reduction of raw material cost, and it may make it easy to contrive a continuous process for large-scale production of CNTs.

In this research, the CCVD method based on CH_4, SiO, and transitional metal catalysts was used, and influences of process parameters on the growth of CNTs were studied. Experimental conditions that lead to highest CNT growth rates will be presented.

2 LITERATURE REVIEW

2. 1 Carbon Nanotubes

2. 1. 1 Fullerenes

The discovery of CNTs arises from the production of carbon clusters, C_n where $1<n<30$ and C_{2n} where $20<n<90$, which have been produced using a laser vaporization of graphite by Rohlfing, et. al. [17]. This research showed that the C_{60} peak in the mass spectra is largest in a range of even number of atoms, for $n>40$. Following this report, Krote and coworkers made it possible to demonstrate the dominance of the C_{60} peak, which is about 40 times larger than neighboring clusters, by increasing a He pulse and the time between vaporization and expansion [1]. Fullerenes are large, closed-cage, carbon clusters and have several special properties that are not found in any other compounds. Consequently, Krote and coworkers described the details of their crystal structure and bond strength at that time, and their stability in the gas phase was proven. Figure 1 shows the structure of the fullerene molecule, C_{60} [18].

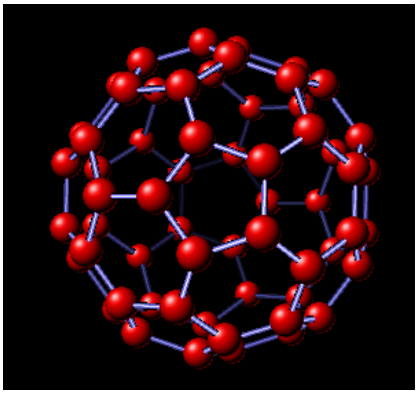

Figure 1 The structure model of fullerene molecule, C_{60} [18].

2. 1. 2 Structure

The bonding, local coordination, and general crystal structure of CNTs are similar to those of fullerenes, but CNTs can greatly extend their length up to more than 10 mm [19]. In addition, CNTs are of cylindrical shells, not the soccer-ball shape, formed by rolling graphene sheets. Figure 2 presents one of the examples of long CNTs synthesized by University of Cincinnati researchers.

Figure 2 An example of long carbon nanotubes [19].

CNTs are classified into single walled carbon nanotubes (SWNTs) and multi walled carbon nanotubes (MWNTs); SWNTs are formed by rolling a single graphene sheet into a cylinder along an (m, n) lattice vector in the graphene sheet, while MWNTs are composed of multiple graphene sheets [20]. Both SWNTs and MWNTs have closed ends where hemispherical units cap the hollow tubes. Figure 3 shows SWNTs and MWNTs respectively [21, 22].

1) 2)

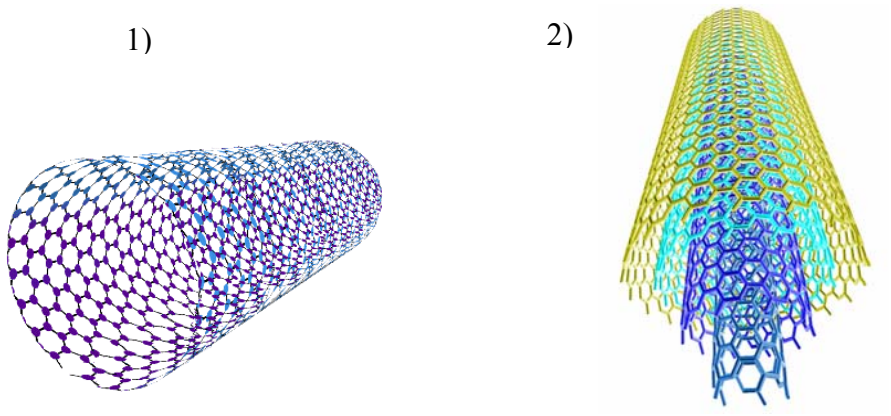

Figure 3. Structures of CNTs; 1) 3-D structure of SWNTs [21]. 2) 3-D structure of MWNTs [22].

Depending on the manner for rolling graphene sheets, the electrical properties of CNTs vary. This manner is defined by chiral vectors, $C_h = na_1 + ma_2$, where n and m are integers and a_1 and a_2 are lattice vectors. CNTs can be either semiconductive or metallic conductive. When the relative orientation of repeating hexagons is in the chair configuration, CNTs represent obviously high electrical conductivity. Figure 4 shows the graphene plane that indicates three orientations of SWNTs. Figure 5 shows different chiral types of SWNTs: armchair, chiral, and zigzag tubes, respectively [23].

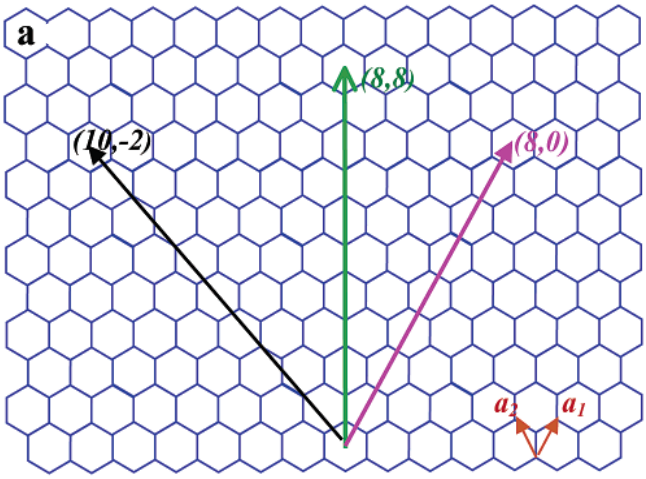

Figure 4 Schematic honeycomb structure of a graphene sheet [23].

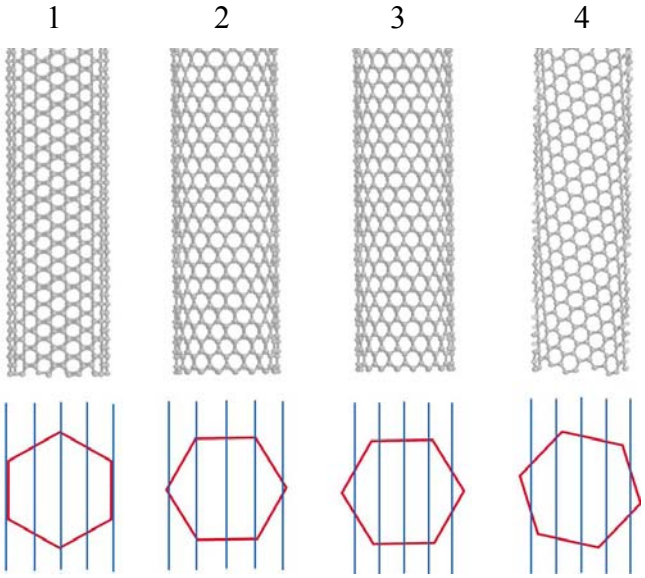

Figure 5. Schematic structure of each type of SWNTs [23];
1) arm-chair type, metallic state, 2) zigzag type, semimetallic-semiconducting state,
3) zigzag type, semiconducting state, 4) chiral type, semiconducting state.

2. 1. 3 Properties

CNTs are hybridized as sp^2 formed by 2*s* and 2*p* orbits, which means the two dimensional structure and shows the highest bond strength among any chemical bonds. In general, 1*s* and *n*-*p* hybrid orbits are denoted as sp^n, and there exist three hybridization types, *sp*, sp^2, and sp^3. Graphite and diamond, as well as CNTs, are also formed by elemental carbons, but each structure and properties are remarkably different. Graphite is a good conductor, and has σ bonds formed from the overlap of sp^2 hybrid orbits. It consists of stacked two dimensional planner layers. Although graphite is hybridized as sp^2 within planner layers, like CNTs, the planes are widely separated from each other indicating weak forces, namely van-der Waals forces. Hence, they are easily slipped depending on the direction of the force added. Diamond is a good electrical insulator, and shows the high thermal conductivity by addition of impurities because its structure efficiently distributes thermal motion in three dimensions. Diamond is hybridized as sp^3 and forms the three dimensional structure with the striking hardness [24, 25].

Various properties of CNTs are determined by their crystal structures. Depending on the types of CNTs, their properties are different. The main properties, electrical conductivity, mechanical strength, chemical reactivity, and optical activity, are described as follows [26-29].

Electrical conductivity in CNTs depends on their molecular structure related to their band structure and band gaps. As mentioned above, the differences in conductivity can be easily derived from the chiral vectors. It was reported that an

(n,m) nanotube is metallic when $n=m$ or $n - m = 3j$, where j is an integer. The resistance to conductivity is determined by quantum mechanical aspects, which is independent of the length of CNTs.

In mechanical strength, CNTs have an extremely high Young's modulus in their axial direction. This arises from the localization of π bonds resulting from the circular curvature of CNTs. CNTs also have the strongest tensile strength associated with sp^2 hybridization. Since CNTs are low density materials, their specific strength is obviously higher than any other materials. Furthermore, the tube diameter of CNTs affects their mechanical strength due to the change in their electronic density.

CNTs are not chemically reactive due to their stable crystal structure. For instance, without any chemical functionalization, CNTs can not be successfully dissolved in solvent or mixed with any solutions. Therefore, the chemical reactivities of SWNTs and MWNTs have been studied [30-33]. In SWNTs, since the π-orbital delocalization caused by increased pyramidalization angles directly influences the chemical reactivity, the sidewall and end caps of SWNTs are distinctive. Furthermore, since the diameter of SWNTs is inversely proportional to the π-orbital delocalization, a smaller tube size is desired to increase the chemical reactivity. Hence, to improve the solubility in any solvents, the curvature needs to be controlled and optimized by chemical modification. In MWNTs, they are less reactive than SWNTs. Therefore, more severe conditions for chemical functionalization or modification of MWNTs are required compared to those for SWNTs. Chemical modification of MWNTs using doping with alkali metals and transition metal halides can induce a charge transfer

between strong intercalated species and MWNTs. Hence, it seems to be useful for enhancement of thermal and electrical conductivities. Chemical functionalization of MWNTs has been studied using conventional heating or microwave irradiation. Consequently, some functionalized MWNTs, such as MWNTs-COOH, MWNTs-NCO, and MWNTs-$(CONH(CH_2)_{17}CH_3)_n$ were obtained. Their termini can improve the dispersiblility of MWNTs in various solutions.

There are many factors that affect optical activities of CNTs, including, for instance, their tube size, length, conformity of composite materials, host materials used for dissolution of CNTs, and their concentration in solution [34-38]. In a view point based on the isogonal symmetries, the tensor of the dielectric permeability ε and optical activity *A* indicate that most of CNTs are optically active, but their optical activities decrease with an increase in tube sizes. Depending on accommodation of the group added to MWNTs, functionalized MWNTs show highly hydrophobic and tend to have relatively strong hydrogen bonds with water molecules in solution. Those interactions affect optical limiting activities.

2. 1. 4 Applications

Current use of CNTs includes composite fibers and automobile parts. In addition to these two needs, there are much more applications of CNTs due to their novel properties resulting from their crystal structures, topologies, and tube size distributions [39-41]. Some future applications of CNTs are presented in Table 1.

Table 1. Future applications of CNTs

Property Group	Applications	Needs
Mechanical	High performance composites (with a polymer, metal, metal oxide, and ceramics)	Reinforcements, Clothes, Nanoprobe/Nanotweezers, Nanoelectronic devices
	Rubber compounds	Tires
	Conductive Plastics	Gears, Wires
Electrical	Conductor/Semiconductor	Transistors, Memory devices, Switches, Integrated circuits, Sensors, Actuator
	Field Emitters	Flat panel displays, X-ray/Microwave generators, Lamps, Gas discharge tubes
Chemical	Larger surface composites	Capacitors, Batteries, Fuel cells

2. 2 Methods for CNT Growth

2. 2. 1 Arc-discharge

Arc-discharge is the first method developed for the synthesis of SWNTs and MWNTs. MWNTs were discovered in 1991 [1], while SWNTs were synthesized using metal catalysts in 1993 [42]. This technique is performed using DC in a helium (He) environment. Two high purity graphite rods are used to produce fullerenes. After arc-discharge for a few minutes, soot containing CNTs is deposited on the cathodic rod, while the anodic rod is continuously consumed. One of the key factors in producing CNTs seems to be the pressure control of He and composition/purity of the graphite rod. In the large-scale production, production rates of 24 mg/min soot containing 48% CNTs and 8 mg/min of SWNTs were reported [3, 4], and the purification process of CNTs from polyhedral graphite particles or encapsulated metal particles seems to be still problematic. The schematic model of this technique is shown in Figure 6 [43].

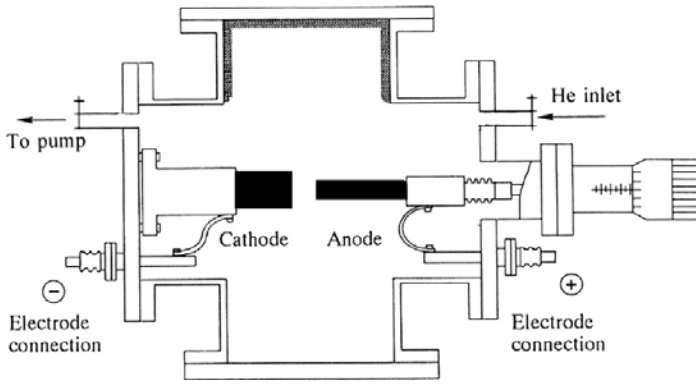

Figure 6. Schematic diagram of arc discharge apparatus [43].

2. 2. 2 Laser vaporization

The laser vaporization technique for the synthesis of SWNTs was reported for the first time by Smalley, et. al. in 1995 [44]. At that time, SWNTs were produced using transition metal/graphite composite rods. Ni and Co were used as catalysts and doped into the graphite [44]. MWNTs can also be synthesized with this technique using pure graphite targets [45]. A pulsed laser, YAG or Nd-YAG, is used to vaporize the graphite targets inside the furnace heated to a temperature of approximately 1200 °C, and an inert gas, such as He and argon (Ar), is used at constant pressure during the reaction. After the vaporized carbons cool down, they condense and form solid carbon clusters through the liquid phase of metals. It is also assumed that transition metals transform from the vapor phase into the liquid phase, and condense together with carbon after metal carbide particles are formed in the liquid phase [46]. The growth of CNTs then starts when metal carbide particles are saturated with carbon. In large-scale production, to achieve a high yield of CNTs, the inert gas condition, the atomization of gas mixture, and the purification process were studied [47, 48]. The ultrasonic filtration, oxidation, acid treatment, annealing, their combination, new targets, and additives to enhance the purification were already reported [49-52]. Figure 7 shows the schematic model of the laser vaporization technique [53].

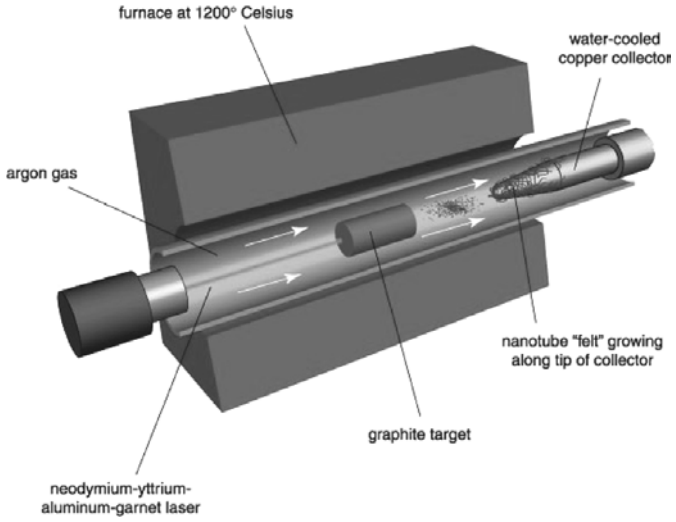

Figure 7. Schematic diagram of laser vaporization apparatus [53]

2. 2. 3 Chemical vapor deposition (CVD)

Chemical vapor deposition (CVD) for the synthesis of CNTs was reported by M. Jose-Yacaman, et. al. in 1993 [54]. CNTs are synthesized by precipitation of gaseous carbon clusters from decomposed hydrocarbons. Gaseous carbon sources catalyzed by transition metals are heated inside a furnace at a temperature of approximately 1000 °C at ambient pressure, and are deposited onto the surface of the catalyst support materials. There are reports on the CNTs synthesis by the catalytic CVD of CH_4 [55,56], C_2H_4 [57-59], benzene (C_6H_6) [60-62], acetylene (C_2H_2) [63, 64], and carbon monoxide (CO) [65-67]. Fe, Co, Ni, Mo, and Y have been studied as transition metal catalysts, while SiO_2, Si, Al_2O_3, MgO, and NaY zeolite [68] have been often used as support materials for catalysts. Depending on the combination of support materials, carbon sources, and transition metal catalysts, pretreatment is sometimes performed using active gases, such as ammonia (NH_3) [69] and hydrogen (H_2) [70].

In addition to the catalytic chemical vapor deposition (CCVD), several different techniques have been reported, including the plasma enhanced CVD [71, 72], aero gel-supported CVD [73, 74], a HiPco method [75, 76], alcohol CCVD [77], laser-assisted thermal CVD [78], a CoMoCat method [79, 80], and Vapor phase growth [81]. Figure 8 shows a schematic model of a typical CCVD reactor [82].

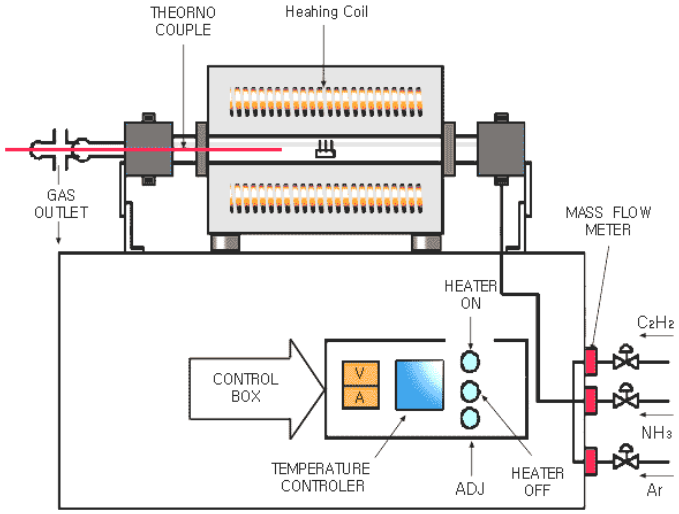

Figure 8. Schematic diagram of catalytic CVD apparatus [82].

2. 3 Growth Parameters

In the chemical vapor deposition (CVD), a hydrocarbon used as carbon sources is one of the most important factors. Among above mentioned hydrocarbons, CH_4 has been focused because of its high stability at elevated temperature and an abundance of natural resources. Kong, et. al. [55] reported the first synthesis of CNTs by the catalytic chemical vapor deposition (CCVD) of CH_4. Other important factors in producing CNTs seem to be activities of transition metal catalysts and operating conditions controlled by process parameters. For instance, in the combination of CVD of CH_4 and Si/Ni composite catalysts, NH_3 greatly affects the orientation of CNTs and enhances the catalyst activity. Vertically-aligned CNTs can be obtained by increasing the ratio of CH_4/NH_3 as well as the feed of NH_3 at a temperature of 900 °C [69].

In the synthesis of SWNTs by the CCVD of CH_4, influences of support materials, the reaction temperature, and the composition of transition metals, as well as the comparison with another carbon source, have been studied. In general, it has been concluded that Al is better than Si as a support material due to its strong interaction with transition metals in the CCVD process of CH_4. The texture properties, such as surface area, porosity, and density of catalysts, also strongly affect the yield of SWNTs [56]. From this view point, a sol-gel method for preparation of catalysts has been studied [83]. Individual SWNTs can be abundantly synthesized using an Fe_2O_3/alumina (Al_2O_3) catalyst at temperature around 1000 °C while bundled SWNTs can be effectively made from an Fe_2O_3/silica (SiO_2) catalyst at the same temperature [55]. Furthermore, it was derived that, in terms of the catalytic activity, Fe_2O_3 is

superior to NiO and CoO [54]. Use of Fe/MgO allows SWNTs to be efficiently synthesized at temperature in the range from 800°C to 900°C due to self-decomposition of CH_4 [84]. In Fe-Mo/MgO, the proportion and quantity of SWNTs decrease with an increase in the reaction temperature [85]. In Fe/SiO_2, C_2H_4 can synthesize individual SWNTs at an extremely lower temperature of 450 °C in comparison to CH_4 [86].

In the production of MWNTs by the CCVD of CH_4, effects of catalytic activities of transition metals, reaction temperature, reaction time, and gas conditions have been often investigated. Regarding the reactivity of transition metal catalysts supported on MgO, when group 8 - 10 series, including the first, second, and third rows, are compared based on the production rate and crystallinity at a temperature of 1000 °C, the amount of MWNTs produced increases in the following order: first (Fe, Co, and Ni) < second (Ru, Rh, and Pd) < third-row metals (Os, Ir, and Pt); and high crystallinities are indicated in the following order: group 10 < group 9 < group 8 [87]. Magnesium oxide (MgO)-supported Fe-Mo and Ni-Y/Mo prepared by the sol-gel method show high yields with a relatively high purity, i.e., 1.5-3.0 g of MWNTs/ 100mg of catalysts in 30 min and maximum impurity of 1.450 wt% [88, 89]. In Ni/Al composite catalysts, the diameter of MWNTs increases but their purity decreases with an increase in the Ni content. In addition, the thermal stability of MWNTs also decreases with increasing Ni contents [90, 91]. In Ni-Cu/Al composite catalysts, the diameter of MWNTs does not change but their average length increases with an increase in the reaction time, and the purity of MWNTs increases but the production

rate decreases when H_2 is used as a carrier gas [92].

2. 4 Issues associated with large-scale production − Purification

As previously mentioned, the catalytic chemical vapor deposition (CCVD) technique can grow CNTs of high quality in comparison to other techniques, and operating conditions can be easily modified and controlled. Therefore, it is desired to produce CNTs as much as possible at low cost. For large-scale production of CNTs, one of serious issues is the process for purification. The products obtained by CCVD mostly contain impurities, including metal catalysts, support materials, amorphous carbon, smaller fullerenes, and graphite. These impurities may reduce mechanical and electrical properties of CNTs, due to the defects of graphene tube walls resulted from impurities. In addition, in order to sufficiently separate CNTs from impurities, some steps need to be repeated, causing a high production cost and a delay of its lead time. Thus, they need to be efficiently removed by suitable treatments. Many removal techniques have been suggested, including an acid treatment, alkaline treatment, oxidative annealing, graphitization, microwave digestion, functionalization, ultrasonication, micro filtration, freezing, and cutting. Some of them are stated as follows.

Acid treatments are used for the removal of transition-metal catalysts, such as Fe, Co, and Ni, as well as that of support materials, MgO, SiO_2, Al_2O_3, and NaY zeolite. Hydrofluoric acid (HF), hydrochloric acid (HCl), nitric acid (HNO_3), sulfuric acid (H_2SO_4), and their combinations are often used [93-97]. One of the procedures in

the acid treatment is, after ultrasonication or oxidation, dissolving the obtained products in acidic solutions to eliminate transition metal catalysts and support materials. Finally, CNTs are filtered, and they are continuously washed with distilled water and/or solvents for pH adjustment.

An alkaline treatment, using sodium hydroxide (NaOH), is considered to be one of ways to remove transition metal catalysts and support materials (Al_2O_3 in particular) at low cost, because of simpler treatment and lower raw material cost compared to acid treatments. There are reports on the purification process of CNTs produced by the CCVD in which Co/NaY zeolite and Co/MgO are used [98]. CNTs are dissolved in NaOH and heated in a range from 600 °C to 800 °C, and they are then washed with HCl, followed by distilled water washing.

The oxidative annealing process can effectively eliminate carbonaceous impurities and clean up the surface of transition metal catalysts. This is due to the difference of reactivities between carbonaceous impurities and CNTs [99]. On the other hand, this treatment tends to remove smaller diameter CNTs, give CNTs some defective damages, or increase the diameter of CNTs [99-101]. Since the diameter of CNTs increases with an increase in the annealing temperature, multiple annealing steps in air are reported, for instance, 225 °C for 18 hr, 425 °C for 1 hr, and 800 °C for 1hr [101].

Graphitization is a heat treatment at high temperature, and it is generally carried out at temperature in the range from 1600 °C to 3000 °C. The advantages of this technique are to remove transition metal catalysts and reduce wall defects of

CNTs [102, 103]. In one of the commercial processes reported, after purging the inside of tubular reactor with nitrogen (N_2), bulk MWNTs are heated up to a temperature of 3000 °C and held for 45 min. After graphitization, the content of Fe catalysts is reduced from 7.1 wt% to less than 0.01 wt% [103]. While this removal process shows practical viability at low cost, it is suggested that influences on physical and mechanical properties of CNTs need to be investigated.

The microwave digestion process is performed using a homogeneous microwave field generated by deal magnetrons of the system. Since the temperature distribution and electric power in this process can be uniformly held, transition metal catalysts can be quickly digested in acid solutions and removed together with carbonaceous materials. As a result, the metal content decreases from 10.39 wt% to 1.03 wt% [104]. In addition, the surface area of CNTs increases with increases in the digestion temperature and time in this process [105]. However, there seem to be somewhat limitations in this process. In case of metals covered by several graphene sheets, they are difficult to be removed. Thus, this technique seems to be useful if the diameter of CNTs is small and CNTs do not cover metals irregularly.

2. 5 Growth Mechanism

Since there are many combinations of transition metal catalysts with support materials and hydrocarbons for the synthesis of CNTs, various studies and discussions have been carried out to investigate the growth mechanism of CNTs,. One of the growth mechanisms suggested by Kataura, et. al. [106] is presented in three steps. First of all, the carbon-containing precursor gas decomposes into carbon clusters, such as fullerenes, and hydrogen, and carbon clusters diffuse to the surface of catalysts. After the chemical reaction or saturation of transition metals with carbon clusters occurs, metal carbides are formed as new catalysts. Finally, CNTs are produced from these metal carbides. Figure 9 presents schematically this growth mechanism of CNTs [106].

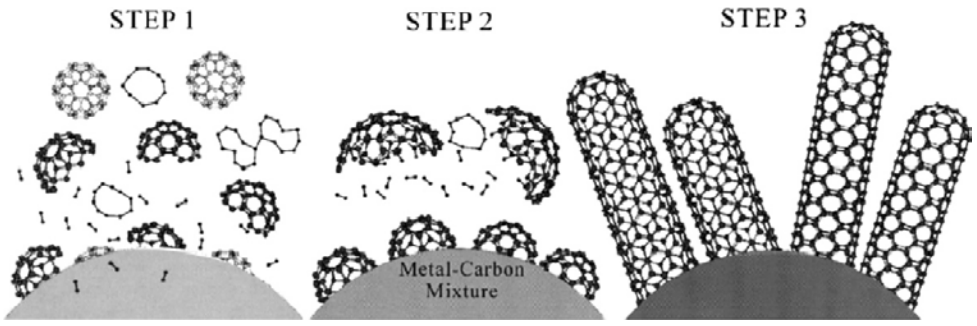

Figure 9. Illustration of steps for CNTs growth [106].

The growth type of CNTs depends on the position of metal particles and is classified into two types: tip-growth and base-growth. In the tip-growth, the metal particles detach from the surface of the support material and move at the tip of growing CNTs. The base-growth (also known as ‘extrusion growth’ or ‘root growth’) occurs when the metal particles remain attached to the support material and CNTs grow upwards from those metal particles. These possible growth types of CNTs are illustrated in Figure 10 [82].

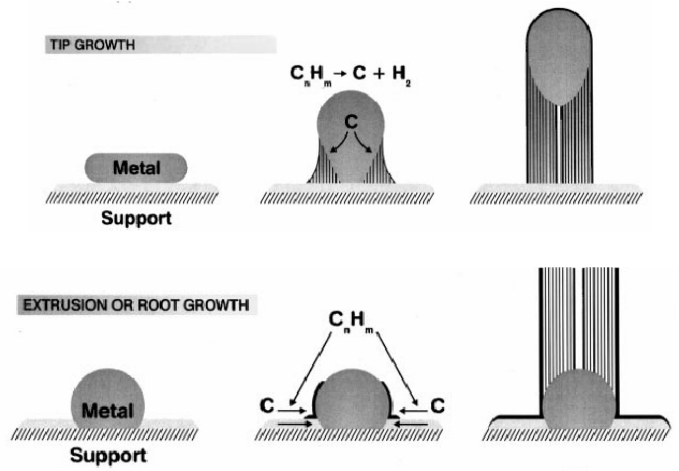

Figure 10. Schematic model of CNTs growth types suggested [82].

3 EXPERIMENTAL

3. 1 CVD System

A horizontal dual alumina-tube reactor (Lindberg sola-basic furnace), 30 mm I.D. and 1500 mm long, was used for the catalytic chemical vapor deposition (CCVD) growth of CNTs in this research. A schematic diagram of the CCVD reactor is shown in Figure 11 (see Appendix A for a picture). Several alumina tubes are inserted inside the external alumina tube. They form a series of internal multiple alumina tubes and prevent the external alumina tube, heated at high temperature, from cracking when a cold alumina sample holder is inserted. A mixture of CH_4 and NH_3 is fed close to the alumina sample holder directly through a 1/4" alumina tube. The inlet of N_2 or Ar is set next to the side of the teflon stopper for purging the whole heated reactor.

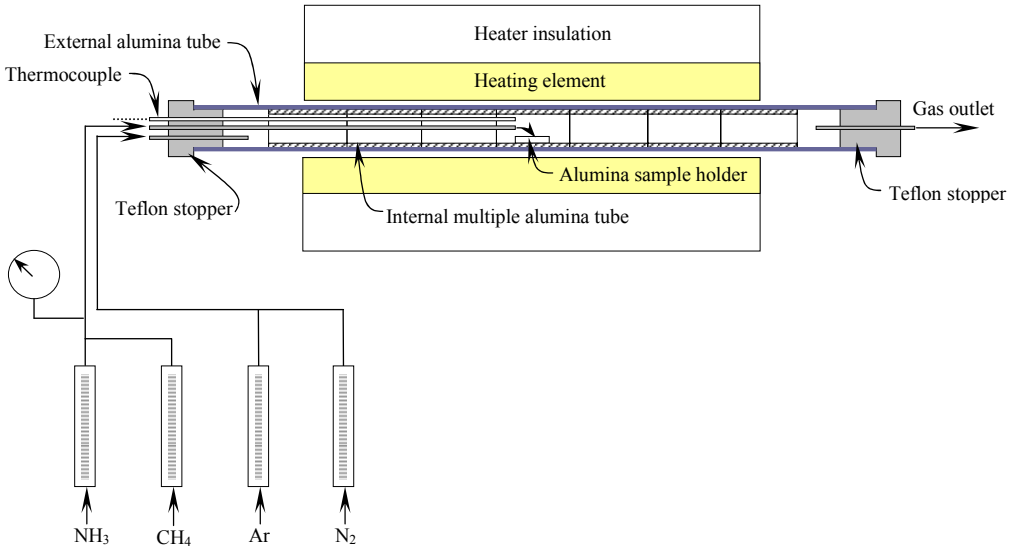

Figure 11. Schematic diagram of catalytic CVD reactor.

3. 2 Materials

The suppliers from which raw materials were purchased or provided are listed in Table 2.

Table 2. Suppliers for raw materials

Material	Suppliers	Purity
SiO (44 μm D)	Sigma-Aldrich Co.	99.99%
SiO (8 μm D)	Sin-Etsu Chemical Co.	—
$Fe(NO_3)_3 \cdot 9H_2O$	Mallinckrodt Co	—
$Ni(NO_3)_2 \cdot 6H_2O$	Sigma-Aldrich Co.	—
Ethanol	Aaper alcohol and chemical Co.	99.99%

3. 3 Catalyst preparation

Two transition metals, Fe and Ni, were focused as catalysts in this research. Ferric nitrate nonahydrate, $Fe(NO_3)_3 \cdot 9H_2O$, and nickel nitrate hexahydrate, $Ni(NO_3)_2 \cdot 6H_2O$, were used as raw materials. They were dissolved in ethanol in a beaker, and the ethanol solution containing these transition metals was then mixed with SiO powders. The content of metals, in grams of transition metals per gram of SiO, was changed in a range of 1 - 13 wt%. The suspension was stirred in the beaker while ethanol was evaporated at 80˚C under atmospheric pressure. The dried materials were ground in a mortar for 1.5 minutes, and the ground powder was placed in an alumina tray and heated in an air stream at temperature in the range from 300˚C to 1100˚C for 2 hours in a tubular flow reactor and then cooled to room temperature. After the oxidation in air, they were ground in a mortar for 0 - 10 minutes. Silicon monoxide (SiO) powders of two different average particle sizes, 8 μm and 44 μm, were used as the supporting substrate for the production of CNTs. Figure 12 shows a sample of catalysts prepared (3 wt% Fe). Table 3 presents the main procedures for the catalyst preparation. Table 4 through Table 7 show catalysts used for this study.

Figure 12. A sample of catalysts prepared (3 wt% Fe).

Table 3. Summary of procedures for catalyst preparation.

Procedure	Conditions	
Raw material	Support	SiO (8 μm D, 44 μm D)
	Metal	$Fe(NO_3)_3 \cdot 9H_2O$, $Ni(NO_3)_2 \cdot 6H_2O$
	Solution	Eethanol (99.99%)
Evaporation	Temperature	80 °C
	Time	4 hr
	Condition	Stirred in atmosphere
Pre-grinding	Time	1.5 min/1.0 - 2.0 g
Oxidation	Temperature	300 - 1100°C
	Time	2 hr
	Condition	Air (1000 cc/min)
Post-Grinding	Time	0 - 10 min /1.0 - 2.0 g

Table 4. Summary of catalysts use for testing effects of particle size of SiO.

metal/support	D/SiO(μm)	oxidation temp.(˚C)	metal/support, g/g
Fe/SiO	44	450	3 wt% Fe
Fe/SiO	8	450	3 wt% Fe
Fe–Ni/SiO	44	450	2 wt% Fe and 1 wt% Ni
Fe–Ni/SiO	8	450	2 wt% Fe and 1 wt% Ni

Table 5. Summary of catalysts for investigating effects of metal composition.

metal/support	D/SiO(μm)	oxidation temp.(˚C)	metal/support, g/g
Fe/SiO	44	450	3 wt% Fe
Fe/SiO	44	450	2 wt% Fe and 1 wt% Ni
Fe/SiO	44	450	1.5 wt% Fe and 1.5 wt% Ni
Fe/SiO	44	450	1 wt% Fe and 2 wt% Ni
Fe/SiO	44	450	3 wt% Ni

Table 6. Summary of catalysts for investigating effects of metal loadings.

metal/support	D/SiO(μm)	oxidation temp.(˚C)	metal/support, g/g
Fe/SiO	44	450	1 wt% Fe
Fe/SiO	44	450	3 wt% Fe
Fe/SiO	44	450	7 wt% Fe
Fe/SiO	44	450	13 wt% Fe
Fe_Ni/SiO	44	450	0.7 wt% Fe and 0.3 wt% Ni
Fe_Ni/SiO	44	450	2 wt% Fe and 1 wt% Ni
Fe_Ni/SiO	44	450	4.7 wt% Fe and 2.3 wt% Ni
Fe_Ni/SiO	44	450	8.7 wt% Fe and 4.3 wt% Ni

Table 7. Summary of catalysts for investigating oxidation temperature effects.

metal/support	D/SiO(μm)	oxidation temp.(˚C)	metal/support, g/g
Fe/SiO	44	450	1 wt% Fe
Fe/SiO	44	600	1 wt% Fe
Fe/SiO	44	750	1 wt% Fe
Fe/SiO	44	900	1 wt% Fe
Fe/SiO	44	1000	1 wt% Fe
Fe/SiO	44	450	3 wt% Fe
Fe/SiO	44	600	3 wt% Fe
Fe/SiO	44	750	3 wt% Fe
Fe/SiO	44	1000	3 wt% Fe
Fe_Ni/SiO	44	300	2 wt% Fe and 1 wt% Ni
Fe_Ni/SiO	44	450	2 wt% Fe and 1 wt% Ni
Fe_Ni/SiO	44	600	2 wt% Fe and 1 wt% Ni
Fe_Ni/SiO	44	900	2 wt% Fe and 1 wt% Ni
Fe_Ni/SiO	44	1100	2 wt% Fe and 1 wt% Ni

3. 4 Synthesis of CNTs

The temperature of the furnace used was set in the range from 900˚C to 1150˚C. Once the inside of the reactor was heated to a prescribed temperature and purged with N_2, an alumina sample holder (25 mm L × 10 mm W × 5 mm H) containing SiO loaded with catalysts was inserted into the reactor. Methane (CH_4) was used as a carbon source while ammonia (NH_3) was used for pretreatment and/or mixing with CH_4. When the pretreatment was performed, NH_3 was first fed at a flow rate of 200 cc/min. The time for the pretreatment was changed in the range from 1 minute to 30 minutes. Following the pretreatment, CNTs were then synthesized by feeding CH_4/NH_3 gas mixtures at a flow rate in the range from 200 cc/min to 650 cc/min. The mass of CNTs grown was measured as the change in the mass of the sample holder between before and after the reaction using a chemical balance. Figure 13 presents catalysts, loaded in an alumina sample holder, and CNTs synthesized in the reaction held in the holder. Table 8 summarizes the major experimental conditions used for the synthesis of CNTs in this research.

When the effects of transition metals on SiO sublimation were studied, NH_3, N_2, or Ar, was fed to metal loaded SiO placed in an alumina sample holder at a flow rate of 200 cc/min at 1000°C. The change in mass of sample holder containing catalyst loaded SiO was measured and compared between before and after the heating.

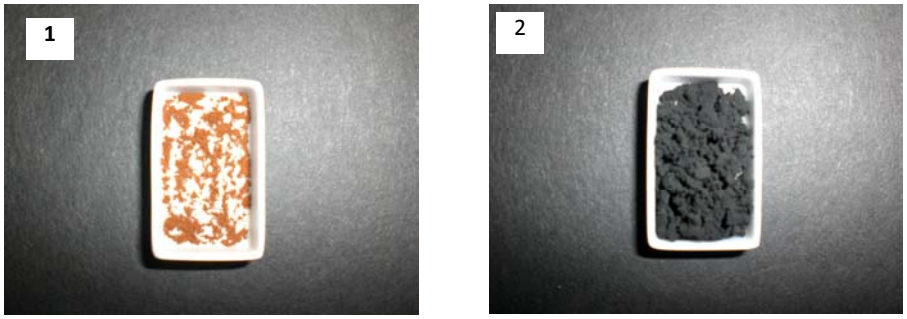

Figure 13. Alumina sample holders; 1) loaded with catalysts, 2) filled with CNTs after the reaction

Table 8. Major experimental conditions

Process	Gas	Flow Rate	Temperature	Time
Pri-Purge	N_2	320 cc/min	1000˚C	10 min
Pretreatment	NH_3	200 cc/min	1000˚C	5 min
Reaction	CH_4/NH_3	450/200 cc/min	1000˚C	5 min
Post-Purge 1	N_2	320 cc/min	1000˚C	5 min
Post-Purge 2	N_2	320 cc/min	1000˚C	3 min

3. 5 Observations

The morphologies of catalysts and CNTs were observed by scanning electron microscopy (SEM). An SEM unit was operated at a rate of 1.2 Hz and exposure time of 13 seconds using PHENOM (FEI Company). The change in mass of sample holder between before and after the reaction was used to quantify a yield. The mass of an alumina sample holder, together with SiO loaded with catalysts, was initially measured using a chemical balance capable of measuring 0.01 mg (Sartorius, Model 2473). After the reaction, the alumina sample holder containing CNTs produced was measured again, and the weight gain was quantified as the amount of CNTs synthesized. It was confirmed that the change in the mass of empty sample holder between before and after the heating was negligibly small. Pictures of the SEM apparatus and chemical balance used in this study are shown in Appendix B.

4 RESULTS

4. 1 Effects of SiO particle size

Figures 14 and 15 show the amount of CNTs synthesized, varying the time for pretreatment. Two different average sizes of SiO, 8 μm and 44 μm, were compared for Fe and Fe-Ni bimetallic catalysts respectively based on the amounts of CNTs synthesized per gram of catalyst in 5 minutes. The catalyst oxidation temperature and reaction temperature as well as grinding conditions were maintained identical.

Two figures indicate essentially the same trend. The growth of CNTs in 5 minutes decreases with an increase in the pretreatment time. Fe-Ni bimetallic catalysts indicate an intermediate peak, and its location varies with the size of SiO particles, as shown in Figure 15. When no NH_3 pretreatment is performed, SiO with an average size of 44 μm demonstrates the maximum CNT yield, in both the single metal and bimetallic catalysts. Single metallic (3 wt% Fe) and bimetallic (2 wt% Fe - 1 wt% Ni) catalysts loaded on 44 μm average sized SiO particles have roughly the same yields of CNTs when used with no NH_3 pretreatment. On the other hand, catalysts loaded on 8 μm average sized SiO particles demonstrate different yields when used with no NH_3 pretreatment, i.e., yields with single metallic catalysts are higher than those with bimetallic catalysts. When the pretreatment is carried out for Fe catalysts for 1 - 8 minutes and Fe-Ni bimetallic catalysts for 3 - 13 minutes, catalysts supported on 8 μm average sized SiO show a larger weight gain than 44 μm average sized SiO.

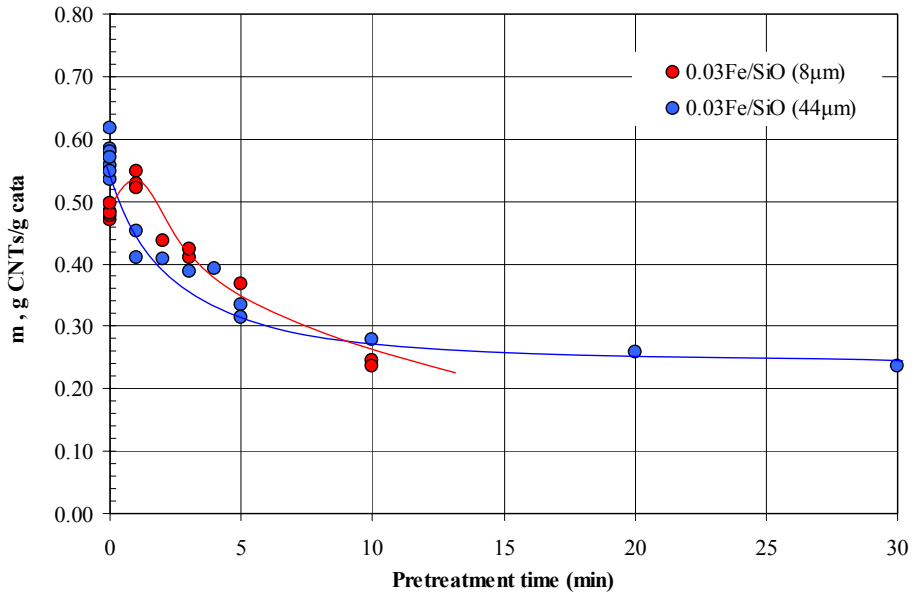

Figure 14. Effects of SiO particle size; Fe (3 wt% Fe), 450˚C oxidation, 1.5 min grinding, NH_3 pretreatment 0 - 30 min, 1000˚C - 5 min reaction.

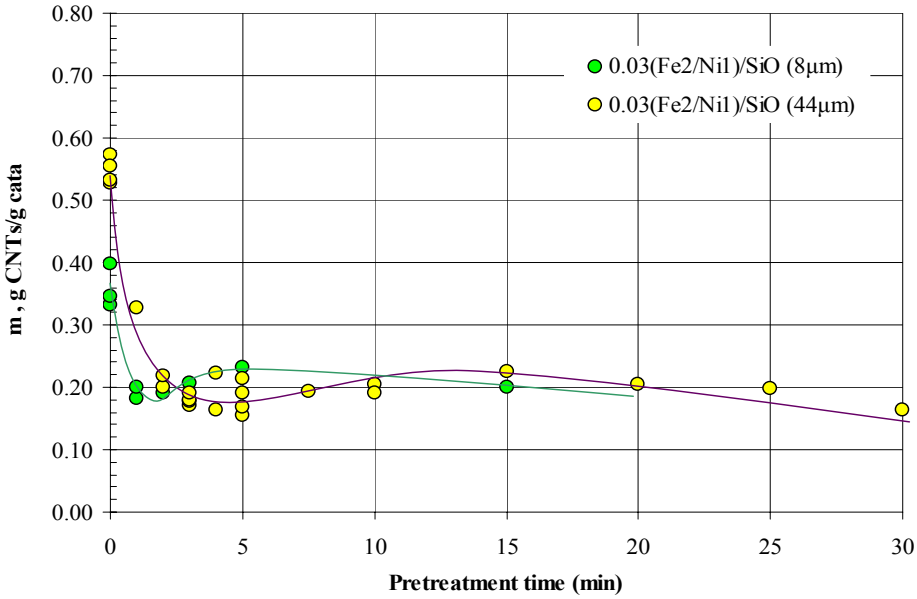

Figure 15. Effects of SiO particle size; Fe-Ni bimetal (2 wt% Fe - 1 wt% Ni), 450˚C oxidation, 1.5 min grinding, NH_3 pretreatment 0 - 30 min, 1000˚C - 5 min reaction.

4. 2 Effects of metal composition

Effects of transition metal compositions on the growth of CNTs were investigated. The total amount of transition metals loaded was fixed at 3 wt% (Fe + Ni = 3 wt%) of SiO mass, as summarized in Table 5. The amount of each Fe and Ni loaded was changed in the range from 0 % to 100 % of the total metal, while the catalyst oxidation temperature and reaction temperature as well as grinding conditions were maintained unchanged. No NH_3 pretreatment was carried out. The average size of SiO particles used is 44 μm.

Figure 16 shows the results based on the mass of CNTs produced per gram of total metals in 5 minutes. The abscissa is represented in terms of the mass fraction of Fe in the total mass of metals loaded. As the fraction of Fe loaded increases, the amount of CNTs produced increases. Catalysts prepared with Fe only (the mass fraction of Fe is 1) yield more CNTs than catalysts prepared with Ni only (the mass fraction of Fe is 0). It is indicated that loading Fe more than approximately 70 percent of the total metal is appropriate in order to achieve high CNT yields. However, loading metals more than 3 wt% a total does not increase the yield of CNTs, as described in the following section.

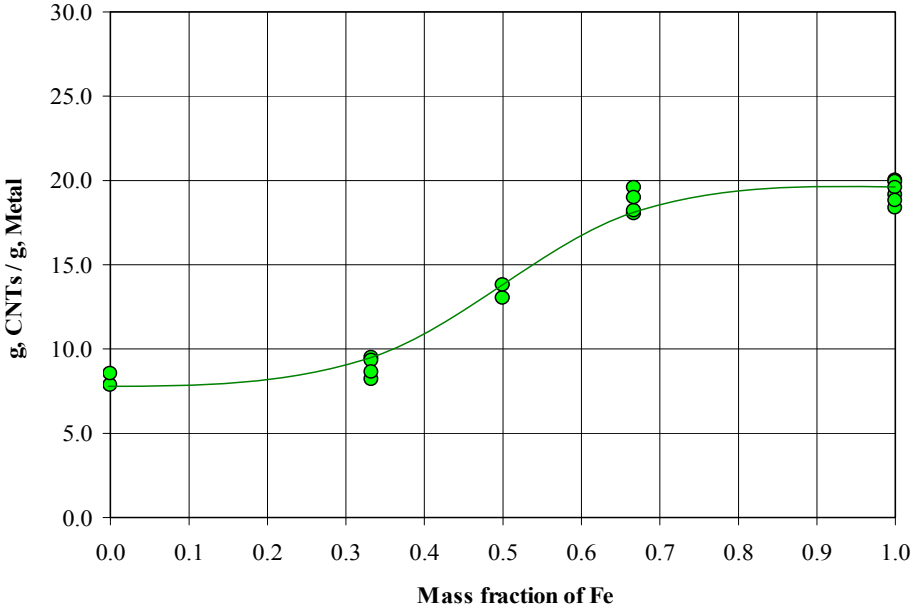

Figure 16. Effects of metal composition; 0.0 = 100% Ni, 1.0 = 100% Fe, 450˚C oxidation, 1.5 min grinding, No NH_3 pretreatment, 1000˚C - 5 min reaction.

4. 3 Effects of metal loading

The total metal loading is another factor that influences the yield of CNTs. Effects of the amount of transition metals were investigated using single metallic and bimetallic catalysts impregnated on 44 μm average sized SiO particles. The ratio of Fe over Ni in the bimetallic catalysts was maintained at 2 to 1. The catalyst oxidation temperature, grinding time, and reaction temperature were all maintained constant, as summarized in Table 6. All the catalysts were used with no NH_3 pretreatment.

Figure 17 shows the results obtained. The mass of CNTs, produced in 5 minutes, per total mass of catalyst metals is used to indicate the efficiency of metal use, rather than a per-catalyst-mass basis. This figure compares two different metal catalysts, Fe single metal and Fe-Ni bimetallic catalysts. When single metallic Fe catalysts are used, an impregnation in the range between 1 wt% Fe and 3 wt% Fe on SiO demonstrates the best efficiency in metal use, and the growth of CNTs per mass of metal decreases with an increase in the metal loading. On the other hand, Fe-Ni bimetallic catalysts show the highest efficiency when the total metal loading is about 3 wt%, and its efficiency decreases with more metal impregnation or less than this. When the total metal loading is about 3 wt%, both the single metallic and bimetallic catalysts yield roughly the same amount of CNTs.

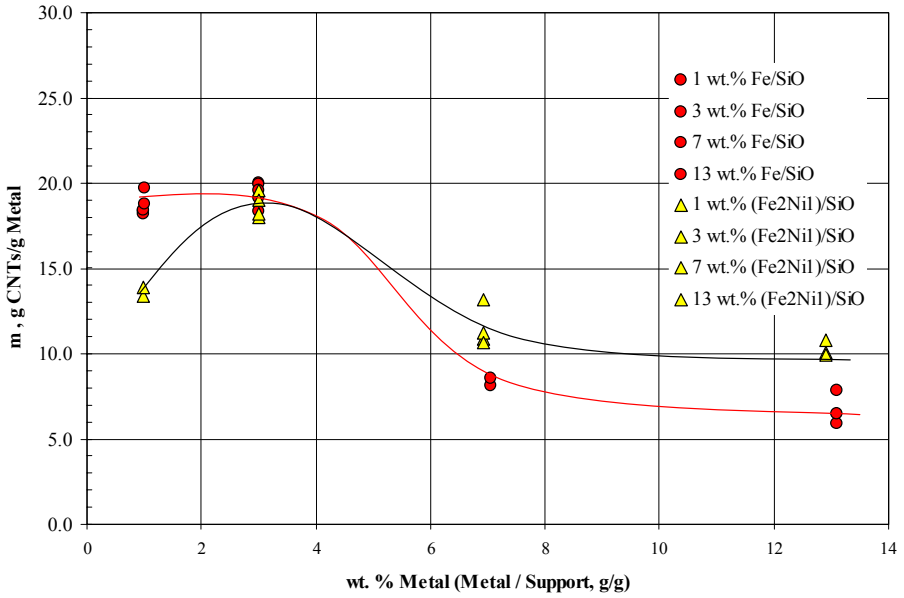

Figure 17. Effects of metal loading; 450˚C oxidation, 1.5 min grinding, No NH_3 pretreatment, 1000˚C - 5 min reaction.

4. 4 Oxidation temperature effects

Figures 18 and 19 show effects of the temperature for catalyst oxidation, based on the amount of CNTs, synthesized in 5 minutes, per mass of catalyst metals, in g CNTs/g metal. In single metallic catalysts, 1 wt% Fe and 3 wt% Fe loadings were tested, while the total metal loading was fixed at 3 wt% for bimetallic Fe-Ni catalysts, maintaining the Fe/Ni mass ratio at 2 to 1. No NH_3 pretreatment was carried out, and the catalyst grinding time was maintained constant. The average size of SiO particles used is 44 μm. The detailed oxidation conditions are summarized in Table 7.

As shown in Figure 18, single metallic Fe catalysts show highest yields of CNTs when oxidized at different temperatures: 600 - 750°C for 1 wt% Fe and 450 - 600°C for 3 wt% Fe, respectively. When the two Fe loadings are compared at these highest yields based on the mass of CNTs produced per mass of metal, a better yield is obtained at a loading of 1 wt% Fe.

On the other hand, as shown in Figure 19, when 3 wt% Fe-Ni bimetallic catalysts are used, high yields of CNTs are observed in the range from 750°C to 900°C. At these highest yields, the mass of CNTs produced per mass of total metals is roughly the same as that achieved with 1 wt% Fe catalysts oxidized in the range from 600°C to 750°C.

Figure 20 shows morphologies of CNTs synthesized on catalysts prepared at different oxidation temperatures. Single metallic catalysts containing 1 wt% Fe, oxidized at 450°C in air, seem to have produced more aligned CNTs, while the other catalysts produce tangled CNTs. Different morphologies of CNTs, namely somewhat

kinkier CNTs, are observed on 3 wt% Fe loaded catalysts prepared at higher oxidation temperature. In some areas of CNTs produced with 3 wt% Fe-Ni bimetallic catalysts oxidized at higher temperature, larger tubes are observed. It is suggested that the diameter of CNTs increases in general with an increase in the oxidation temperature. Some more SEM pictures are presented in Appendix C.

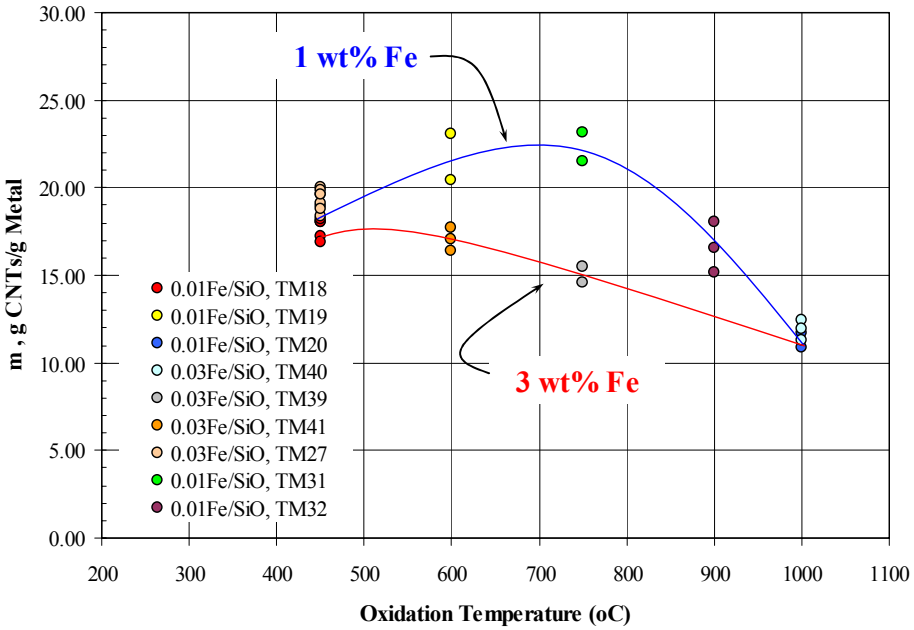

Figure 18. Oxidation temperature effects; Fe (1 wt% Fe, 3 wt% Fe), 1.5 min grinding, No NH_3 pretreatment, 1000˚C - 5 min reaction.

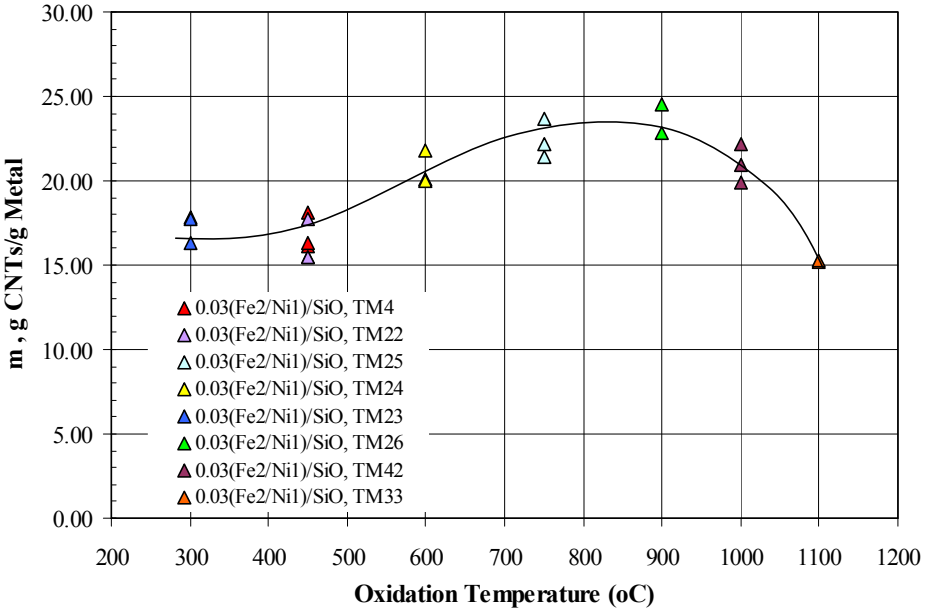

Figure 19. Oxidation temperature effects; Fe-Ni bimetal (2 wt% Fe - 1 wt% Ni), 1.5 min grinding, No NH_3 pretreatment, 1000˚C - 5 min reaction.

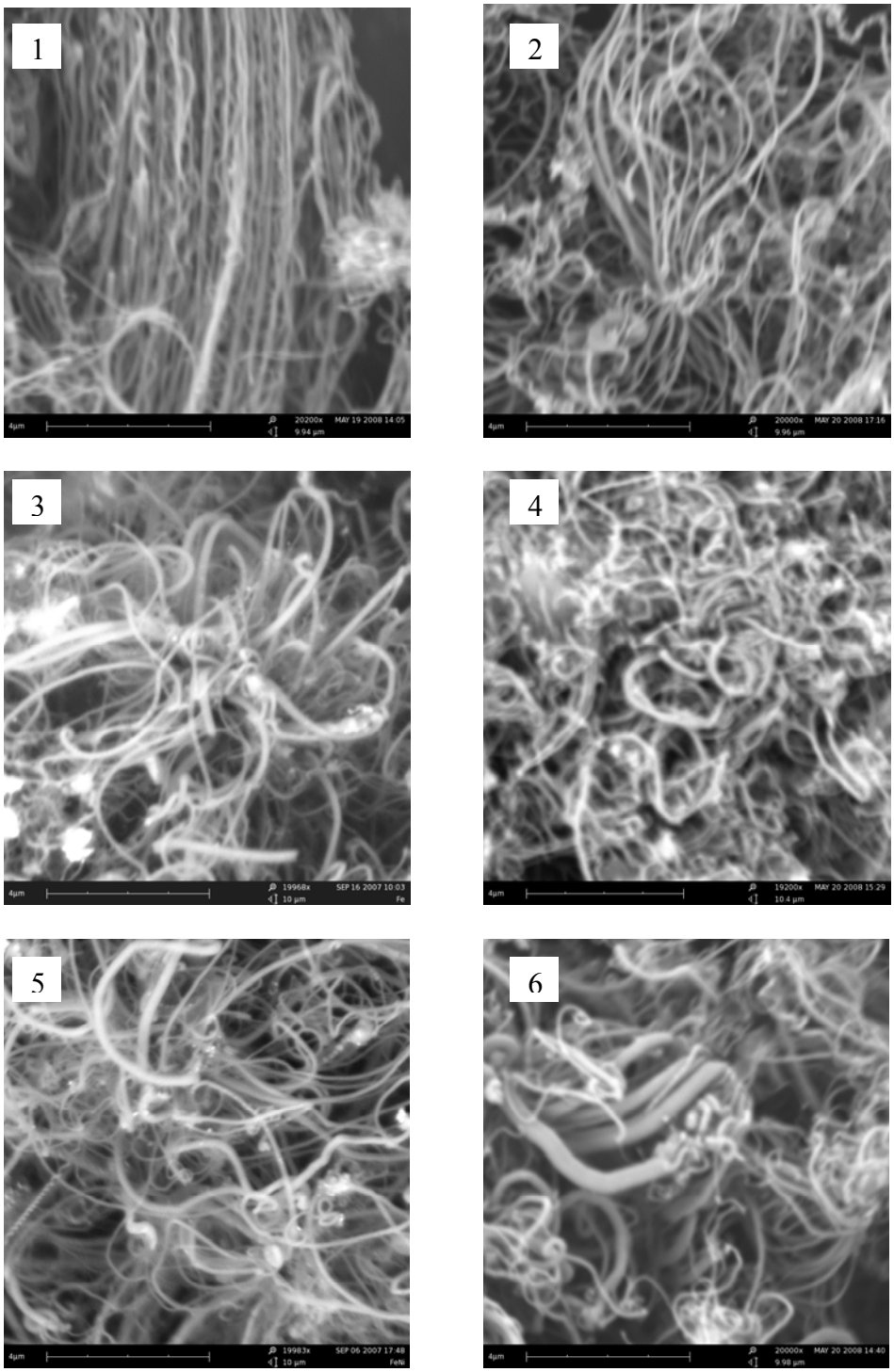

Figure 20. SEM images of CNTs; 1) 1 wt% Fe, 450°C; 2) 1 wt% Fe, 750°C; 3) 3 wt% Fe, 450°C; 4) 3 wt% Fe, 600°C; 5) 2 wt% Fe - 1 wt% Ni, 450˚C; 6) 2 wt% Fe - 1 wt% Ni, 900˚C.

4. 5 Effects of grinding

Figure 21 shows effects of catalyst grinding on the growth of CNTs, taking the mass of CNTs produced per gram of catalysts in 5 minutes as the basis. The catalysts used are single metallic catalysts containing 3 wt% Fe on 44 μm average sized SiO particles. The catalyst oxidation temperature was fixed at 450°C, and no NH_3 pretreatment was carried out.

Grinding catalysts after oxidation seems to be effective for the growth of CNTs. When grinding is performed, the growth of CNTs in 5 minutes increases by about 40 percent, compared to the catalyst used with no grinding. Grinding for 3 minutes seems to be sufficient, because longer grinding does not increase the catalyst activity.

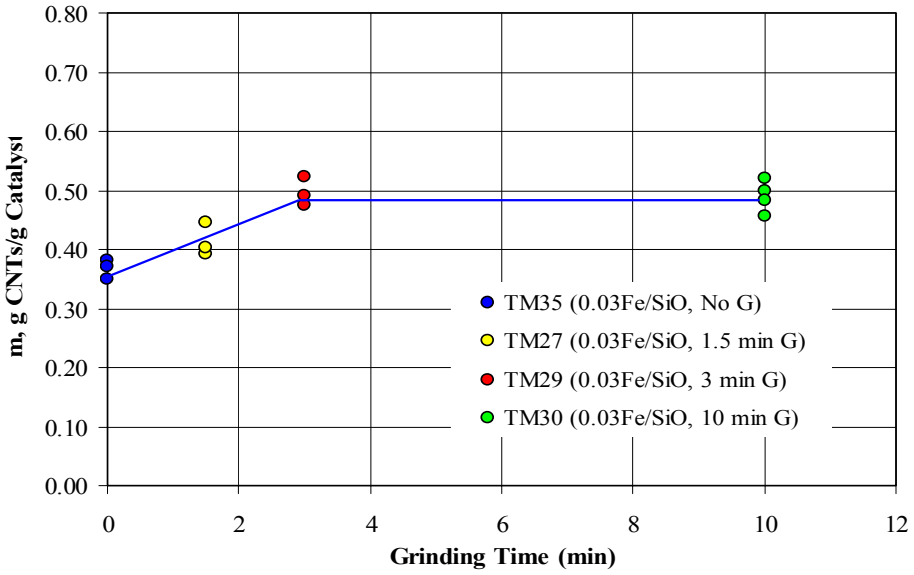

Figure 21. Effects of grinding; Fe (3 wt% Fe), 450˚C oxidation, 0 - 10.0 min grinding, No NH_3 pretreatment, 1000˚C - 5 min reaction.

4. 6 Effects of ammonia pretreatment

Effects of pretreatment in NH_3 on the CNT growth rate have been discussed in conjunction with particle sizes of SiO in an earlier section. Figure 22 shows influences of the NH_3 pretreatment on the growth of CNTs, using catalysts containing 3 wt% total metals at different compositions, based on the amount of CNTs grown in 5 minutes. The oxidation temperature was fixed at 450°C, and 1.5 minutes grinding was done before use of catalysts. The average size of SiO particles used is 44 μm.

The highest activity is always achieved when no NH_3 pretreatment is carried out, regardless of the composition of metals. The catalyst containing 3 wt% Fe maintains highest activities for the growth of CNTs for any pretreatment time investigated. The activity of single metallic Ni catalysts is dramatically reduced by the NH_3 pretreatment. Though the activity of bimetallic catalysts containing Ni drops once due to the NH_3 pretreatment, it recovers with an increase in the pretreatment time. When Ni is mixed with Fe at weight % ratios of 1 Ni/2 Fe and 2 Ni/1 Fe, intermediate peaks appear at about 15 minutes and 10 minutes, respectively.

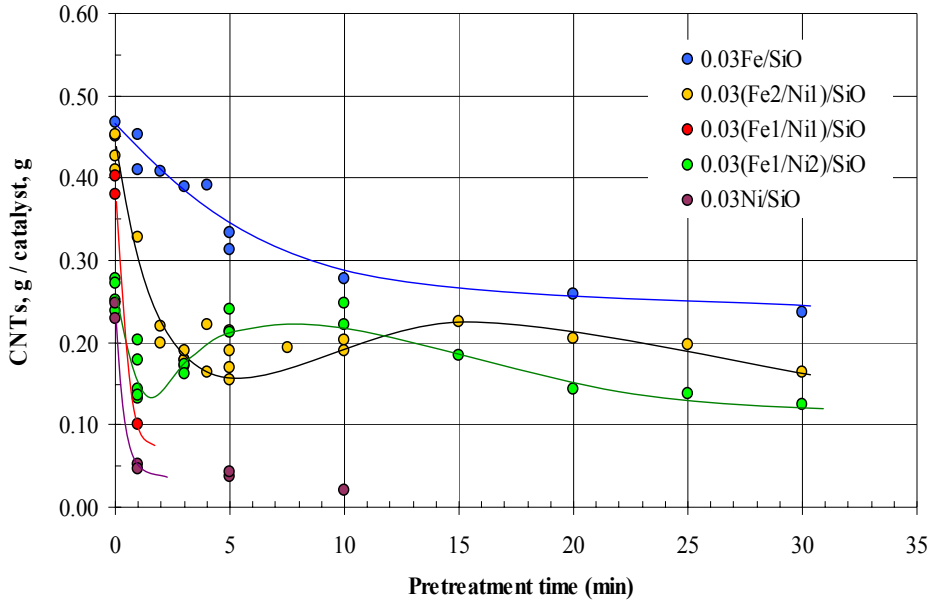

Figure 22. Effects of NH_3 pretreatment; 450˚C oxidation, 1.5 min grinding, NH_3 pretreatment 0 - 30 min, 1000˚C - 5 min reaction.

Figures 23 and 24 compare SEM images of CNTs grown on non-pretreated catalysts to those on catalysts pretreated for 5 minutes. It is observed that the number of large SiO particles, shown as white dots, decreases after the NH_3 pretreatment.

Figures 25 and 26 compare SEM images of catalysts, before and after the NH_3 pretreatment as well as after the CVD reaction, in order to see any effects of NH_3 pretreatment on SiO exterior surface. Catalysts with two different metal compositions were used. Large gray areas indicate SiO particles. There appear to be agglomerations of small clusters on the surface of SiO in some areas after the NH_3 pretreatment. After the CVD reaction, the SiO surface becomes very complex. A higher magnification will be necessary for more detailed observations.

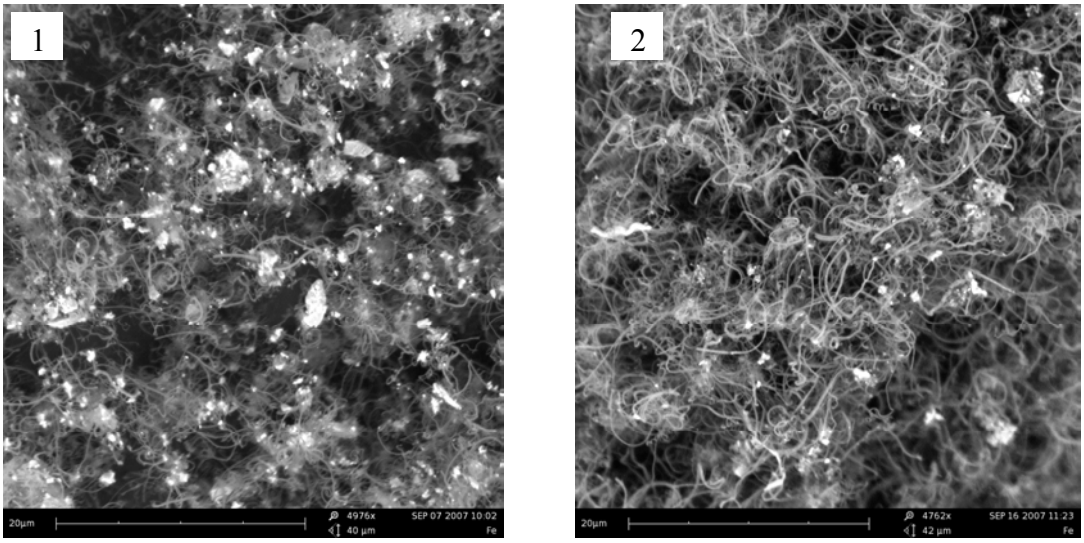

Figure 23. SEM images of CNTs; 3 wt% Fe, 450˚C oxidation, 1.5 min grinding, 1000˚C - 5 min reaction. 1) no NH_3 pretreatment. 2) 5min NH_3 pretreatment.

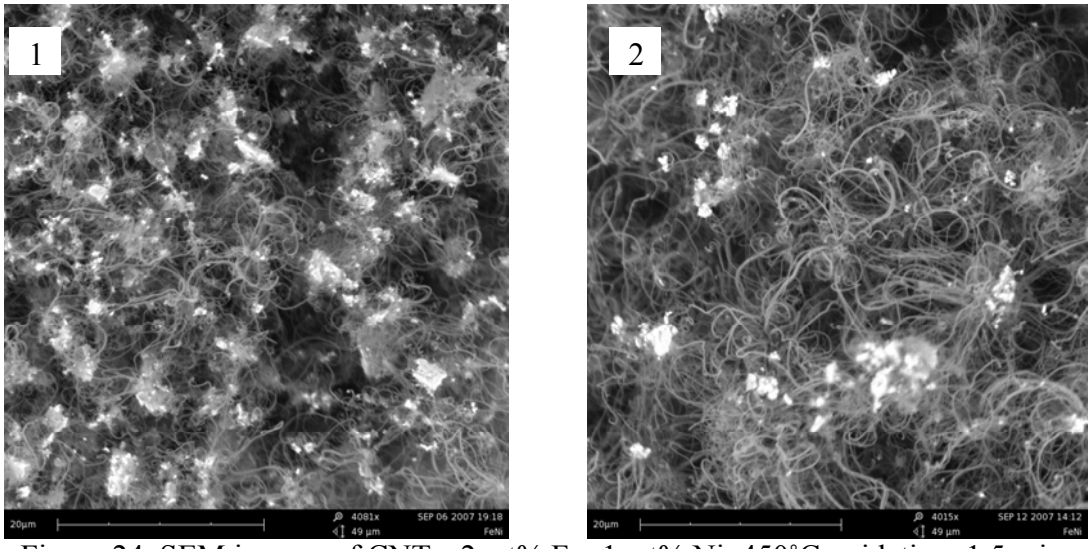

Figure 24. SEM images of CNTs; 2 wt% Fe -1 wt% Ni, 450˚C oxidation, 1.5 min grinding, 1000˚C - 5 min reaction. 1) no NH_3 pretreatment. 2) 5min NH_3 pretreatment.

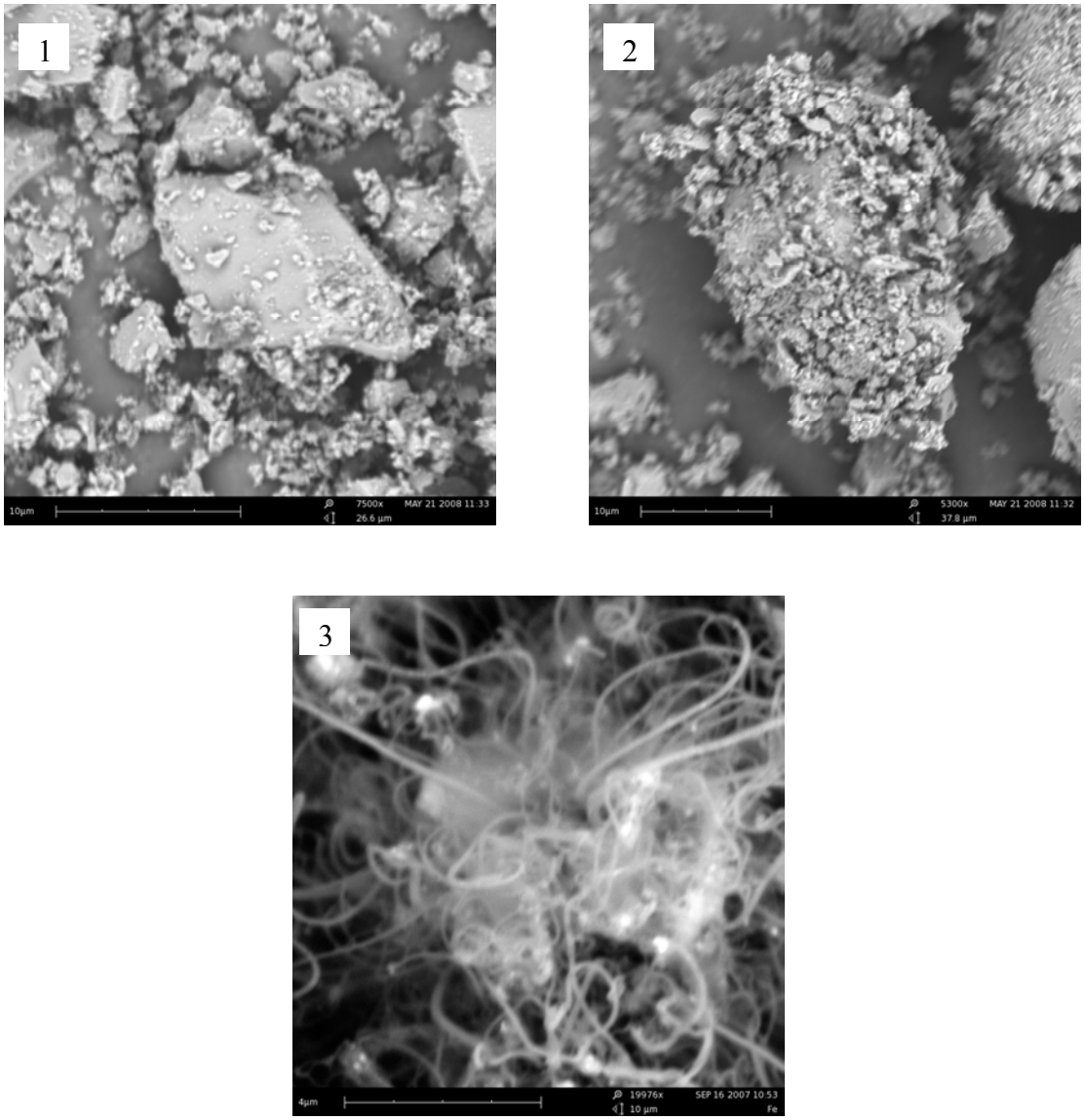

Figure 25. SEM images of catalysts; 3 wt% Fe, 450˚C oxidation, no grinding.
1) before NH_3 pretreatment. 2) after NH_3 pretreatment. 3) after CVD

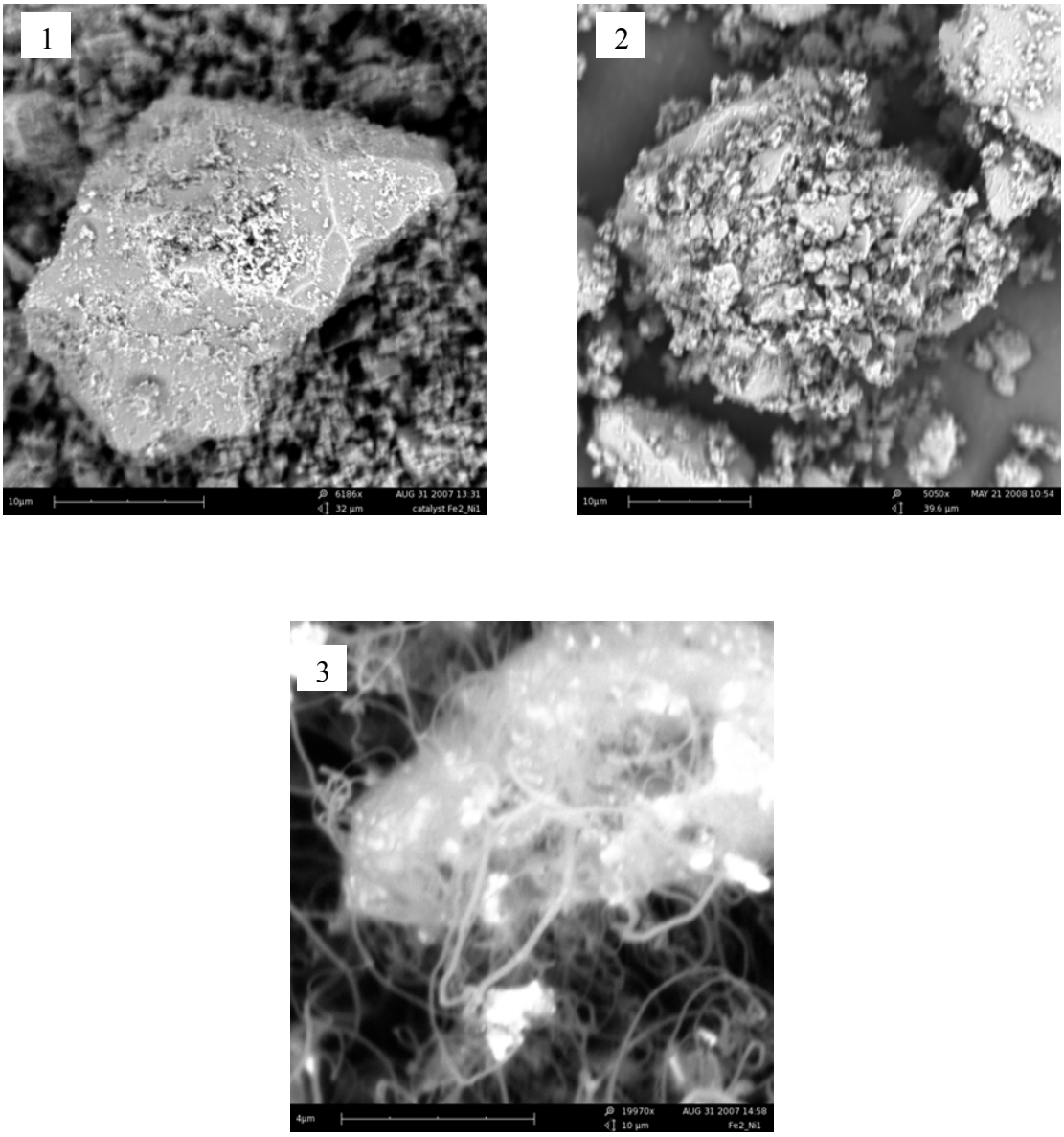

Figure 26. SEM images of catalysts; 2 wt% Fe - 1 wt% Ni, 450˚C oxidation, no grinding. 1) before NH_3 pretreatment. 2) after NH_3 pretreatment. 3) after CVD

4. 7 Effects of reaction temperature

Figures 27 and 28 show effects of the reaction temperature, based on the performance (mass of CNTs synthesized in 5 minutes) of two different catalysts, Fe and Fe-Ni bimetallic catalysts. Both the catalysts contain 3 wt% total metals. The catalyst oxidation temperature was set at 450°C, and the grinding time was 1.5 minutes. Both the catalysts were used without the NH_3 pretreatment.

It should be mentioned that the temperature measurements changed with reaction time, dropping a few degrees C at the beginning when a sample holder was inserted, gradually increasing, and overshooting a few degrees C higher than the prescribed temperature due to the delay of controlling mechanism. The reaction temperature was hence evaluated as an average between the initial and final temperatures during the reaction. The mass of CNTs produced in the 5 minutes reaction became highest at about 1000°C in both the catalysts. It may be concluded, from these results, that the optimum temperature for the growth of CNTs on both the catalysts lie in a range of 990-1000˚C.

The reaction temperature also influenced the morphology of CNTs. Figures 29 and 30 show SEM images of CNTs synthesized at different reaction temperatures. It is indicated that the diameter of CNTs synthesized at higher temperature is larger. Though the effects of reaction temperature on the average CNT diameter have not been clarified yet, it is implied that the reaction temperature has great influences on the sizes of CNTs produced. Further study is needed.

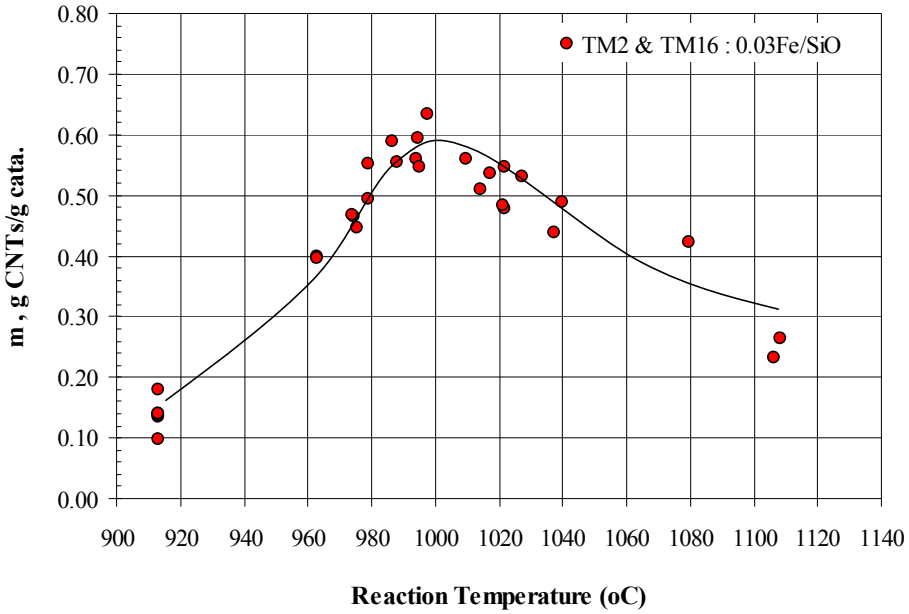

Figure 27. Effects of reaction temperature; Fe (3 wt% Fe), 450°C oxidation, 1.5 min grinding, No NH_3 pretreatment, 5min reaction.

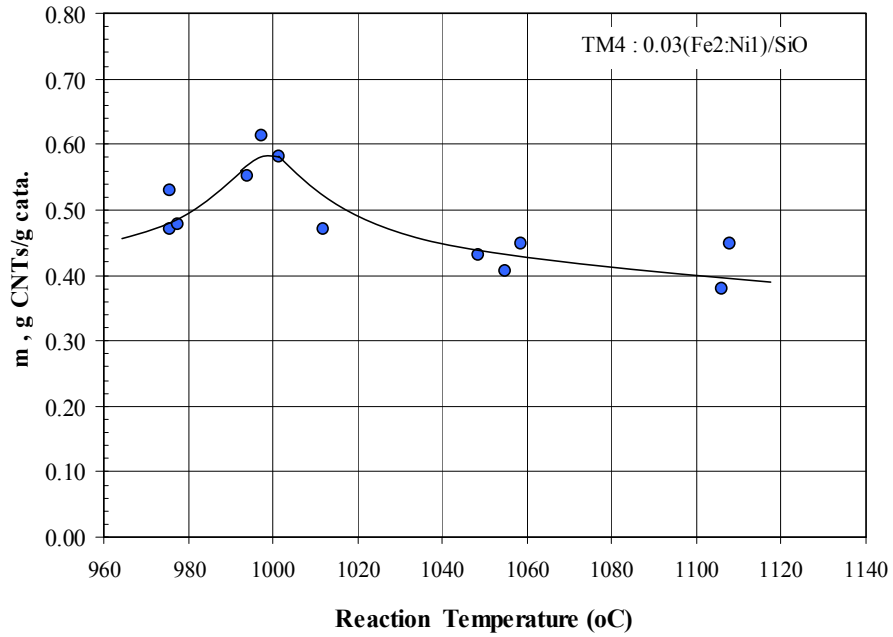

Figure 28. Effects of reaction temperature; Fe-Ni bimetal (2 wt% Fe - 1 wt% Ni), 450°C oxidation, 1.5 min grinding, No NH_3 pretreatment, 5min reaction.

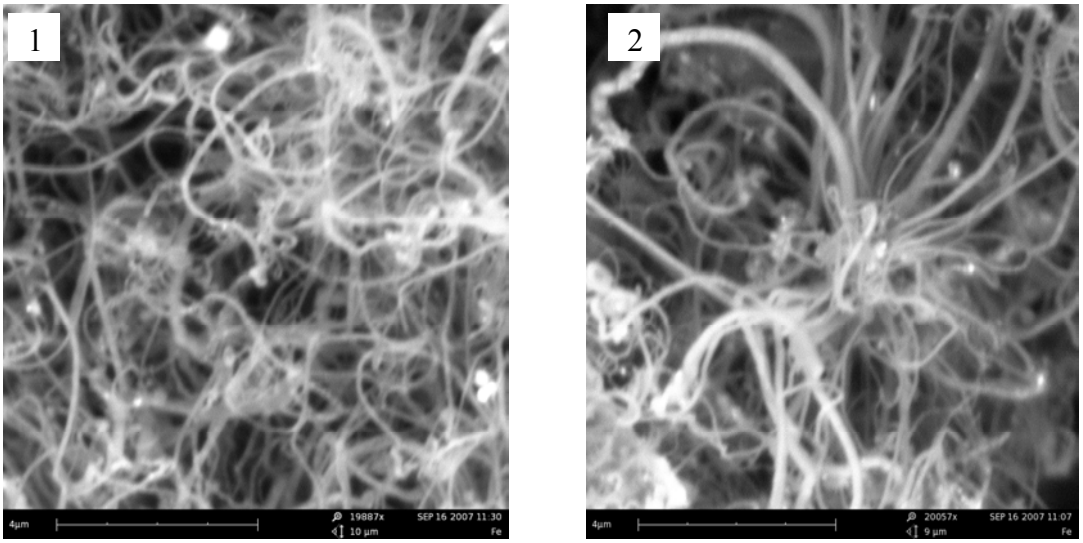

Figure 29. SEM images of CNTs; 3 wt% Fe, 450°C oxidation, 1.5 min grinding, no NH_3 pretreatment, 5 min reaction. 1) 1000°C reaction. 2) 1050°C reaction.

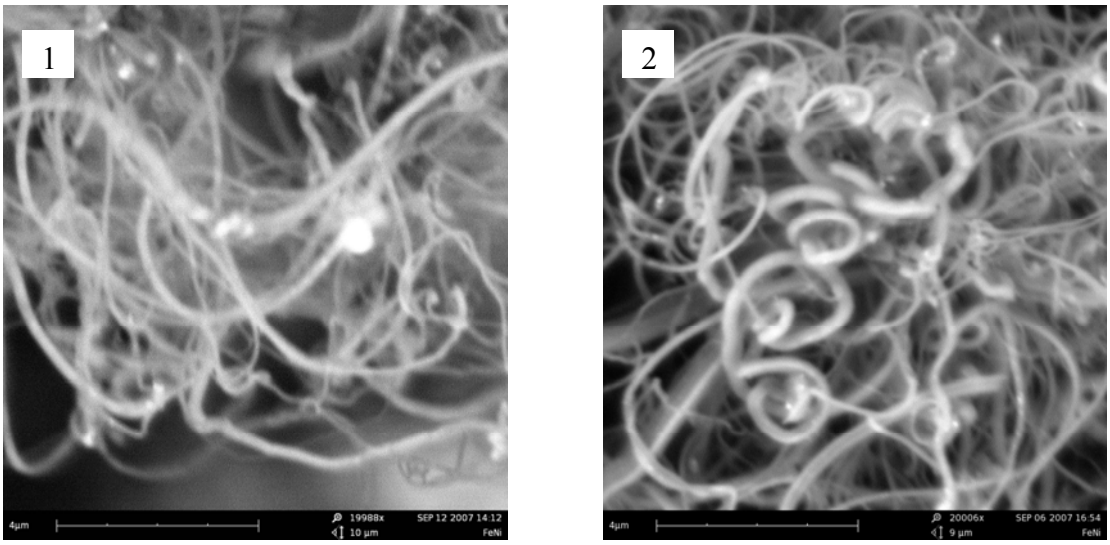

Figure 30. SEM images of CNTs; Fe-Ni bimetal (2 wt% Fe - 1 wt% Ni), 450˚C oxidation, 1.5 min grinding, no NH_3 pretreatment, 5 min reaction. 1) 1000˚C reaction. 2) 1050˚C reaction.

4. 8 Reaction time dependencies

Though the mechanism of changes in the catalyst activity for the CNT growth is not known well, it is common that the catalyst activity changes during the course of reaction. The catalysts used in this research are not exceptions. Figure 31 shows the growth of CNTs with reaction time, when two different catalysts impregnated on 44 μm average-sized SiO particles were used for the reaction at 1000°C: Fe and Fe-Ni bimetallic catalysts. The catalyst oxidation temperature was 450°C, and no NH_3 pretreatment was performed for both the catalysts.

The growth rates of CNTs, represented by the slope of the individual curves, decrease with the reaction time. The trends in the two catalysts are essentially the same, though the activity of the single metallic Fe catalyst lasts longer than that of the Fe-Ni bimetallic catalyst. During the initial stage, on the other hand, the growth on the single metallic Fe catalyst slows down in 5minutes after the initiation of the CCVD reaction, while that on the Fe-Ni bimetallic catalyst quickly slows down in a few minutes and levels off. There appears to be no linear relationship that lasts during the entire course of reaction in both the Fe and Fe-Ni bimetallic catalysts.

When a reactor is continuously operated, the mean residence time of catalysts in the reactor is one of the important operating parameters. When the catalyst activity changes with reaction time, such as the behaviors of the catalysts used in this research, it is important to know the optimum reaction time in order to design and operate the reactor under optimum conditions in terms of the production rate and product morphology. The change in CNT morphologies with the reaction time also needs to be

investigated.

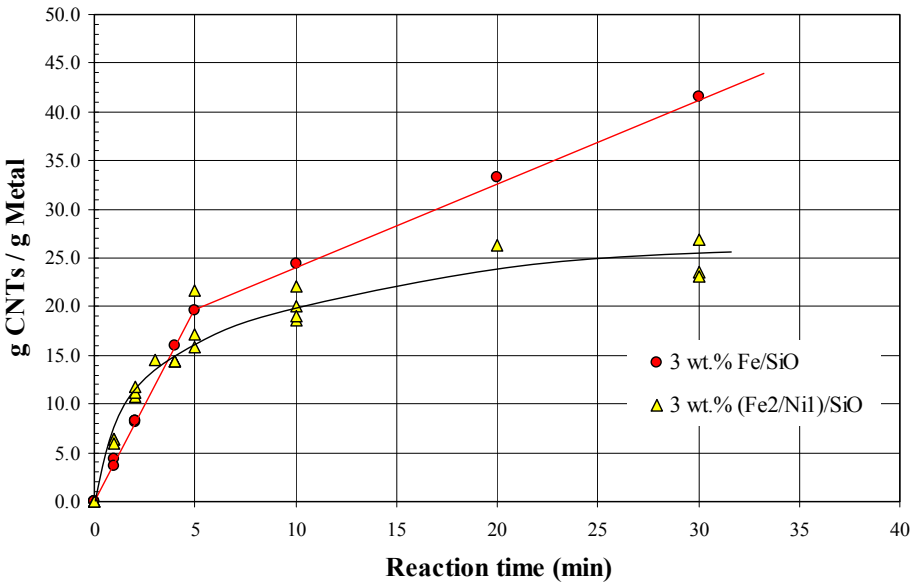

Figure 31. Growth rate changing with reaction time; Fe (3 wt% Fe) and Fe-Ni bimetal (2 wt% Fe-1 wt% Ni), 450°C oxidation, 1.5 min grinding, no NH_3 pretreatment, 1000˚C reaction.

4. 9 Effects of NH_3/CH_4 feed ratio

It has been known that NH_3 greatly affects the orientation of CNTs and enhances the catalyst activity [68]. It has been already shown in an earlier section, using two types of catalysts, that the NH_3 pretreatment rather decreases the activities of the catalysts used in this research. On the other hand, however, the CNTs did not grow appreciably when NH_3 did not coexist with CH_4.

Figure 32 shows the growth of CNTs in 5 minutes versus NH_3/CH_4 feed ratios based on the performance of 3 wt% Fe single metal catalysts. When no NH_3 is fed, the amount of CNTs produced is extremely small. An NH_3/CH_4 feed ratio of 0.15 - 0.25 seems to yield the maximum amount of CNTs. Above a feed ratio of 0.25, the growth gradually decreases. It is evident that NH_3 is indispensable for the growth of CNTs. However, the decrease in the amount of CNTs with an increase in the NH_3/CH_4 ratio seems to be attributed to the CH_4 deficient reaction environment. It will be important to know how the growth of CNTs depends on the CH_4 concentration when the NH_3 concentration is maintained constant and also on the NH_3 concentration when the CH_4 concentration is maintained constant. Concentration dependencies of CNT growth rate need to be investigated in more detail.

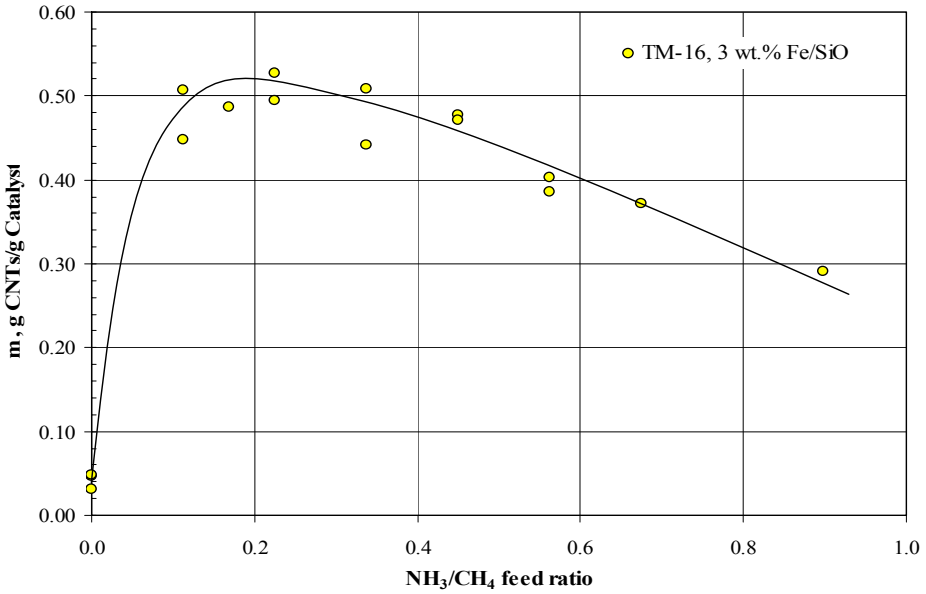

Figure 32. Effects of NH_3; Fe (3 wt% Fe), 450°C oxidation, 1.5 min grinding, no NH_3 pretreatment, 1000°C - 5min reaction.

5. DISCUSSION

5. 1 Growth studies

Several reaction mechanisms could be suggested. One of possible reaction paths with no NH_3 pretreatment is described in the following sections.

5. 1. 1 Dehydration and oxidation in air

It is assumed that nano-sized iron oxide and iron-nickel binary oxide particles are formed by hydration and oxidation of raw materials and adhere to the surface of SiO chemically and physically [107, 108], as shown below.

$$Fe(NO_3)_3 \cdot 9H_2O \rightarrow \alpha\text{–}Fe_2O_3 \ (< 450^{\circ}C\ )$$

$$\rightarrow \gamma\text{–}Fe_2O_3 \ (450 - 500^{\circ}C \text{ or higher}) \ [107]$$

$$Ni(NO_3)_2 \cdot 6H_2O \rightarrow Ni(NO_3)_2 \cdot 2H_2O + 4H_2O$$

$$\rightarrow Ni_{1-x}O + 2HNO_3 + O_2 \ (\ 650^{\circ}C) \ [108]$$

5. 1. 2 Reduction and reoxidation in air

Since Si has a higher electronic nuclear charge than Fe and Ni, it may be suggested that these metals and their oxides are reduced into lower valence metals (e.g. $Fe^{3+} \rightarrow Fe$, $Ni^{2+} \rightarrow Ni$) or oxides (e.g. $\gamma - Fe_2O_3 \rightarrow Fe_3O_4$) by SiO at elevated temperature [109, 110]. On the other hand, because iron oxides, such as *fcc* magnetite Fe_3O_4, are very sensitive to O_2, they may be re-oxidized by amorphous silica SiO_2 or in air, changing their crystal structures, and consequently redox reactions may occur.

$Fe^{3+} \rightarrow Fe^{2+}$: $3(\gamma - Fe_2O_3) + SiO \leftrightarrow 2Fe_3O_4 + SiO_2$ [109]

$Fe^{3+} \rightarrow Fe$: $(\gamma - Fe_2O_3) + 3SiO \leftrightarrow 2Fe + 3SiO_2$ (850˚C) [110]

$Ni^{2+} \rightarrow Ni$: $Ni_{1-x}O + SiO \leftrightarrow Ni + SiO_2$ (at x = 0)

5. 1. 3 Transformation

There are reports suggesting that iron oxides react with SiO_2 and transform into silica containing oxides $(Fe,Si)_xO_y$, such as iron silicate Fe_2SiO_4 (fayalite) at a temperature of 700 - 1100˚C [111-114]. Thus, it is expected that the heat treatment in air results in $(Fe,Si)_xO_y$ and $(Fe,Ni,Si)_xO_y$ at temperature in the range of 700 - 1100˚C. At temperature below 700˚C, it is suggested that less silica-rich iron oxides are formed. Formation of oxides containing silica at higher temperature in the range of 700 - 1100˚C depends on the diffusivity of silica. Possible transformations could be represented as follows:

$Fe_xO_y + SiO_2 \rightarrow (Fe,Si)_xO_y + xO_2$ (900˚C) [111-114]

$(Fe,Ni)_xO_y + xSiO_2 \rightarrow (Fe,Ni,Si)_xO_y + xO_2$

$(\gamma - Fe) + SiO_2 \rightarrow (Fe,Si)_xO_y$

$(Fe,Ni) + SiO_2 \rightarrow (Fe,Ni,Si)_xO_y$

5. 1. 4 Catalytic thermal decomposition of CH_4 and NH_3

In the CVD process, it is reported that CH_4 and NH_3 are decomposed at temperature above 400˚C and 800˚C, respectively [115, 116]. The thermal decomposition of CH_4 and NH_3 generates C and activated N_2, respectively, which work as strong reducing agents to transition metal oxides.

$CH_4 \rightarrow C + 2H_2$ (400 - 500˚C or higher) [115]

$NH_3 \rightarrow 0.5N_2 + 1.5H_2$ (800˚C or higher) [116]

5. 1. 5 Nitrocarburization and refinement

In this light, the introduction of C and N_2 into $(Fe,Si)_xO_y$ and $(Fe,Ni,Si)_xO_y$

suggests three possible reactions, nitrocarburization, nitridation, and curbrization in addition to the formation of transition metal carbonitirdes, $(Fe,Si)_x(C,N)_{1-y}$ and $(Fe,Ni,Si)_x(C,N)_{1-y}$. Since the electronic affinities of C and N_2 for iron oxides seem to be on the same order of magnitudes, nitridation and curbrization occur reversibly through nitrocarburization [117-119]. Nitridation and curbrization of γ–Fe arise at temperature above 900˚C, and they result in the refinement and distortion of crystal structures due to their penetration into the iron-atom lattice [113, 114, 117]. Hence, it is considered that nitrocarburization, nitridation, and curbrization result in refinement of metal carbonitrides, which causes a decrease in the metal particle size. In addition, since activated N_2 derived from NH_3 has much stronger effects on its penetration into and the expansion of the crystal structure than C, it is suggested that the feed condition of NH_3 would be one of the most important factors in the aspect of the crystal structure, as well as effects on the orientation of CNTs. These steps may be summarized as follows:

$$(Fe,Si)_xO_y + C_{1-y} + 0.5N_{2(1-y)} \rightarrow (Fe,Si)_x(C,N)_{1-y} + 0.5O_{2y}\ (600^\circ C - 1200^\circ C)\ [117\text{-}119]$$

$$(Fe,Ni,Si)_xO_y + C_{1-y} + 0.5N_{2(1-y)} \rightarrow (Fe,Ni,Si)_x(C,N)_{1-y} + 0.5O_{2y}$$

5. 1. 6 Metal dusting

Metal carbonitrides are generally unstable and decompose into metal nitrides or metal carbides at temperature above 450˚C [117]. Iron nitrides, such as Fe_2N and Fe_4N, are also thermally unstable, and the release of N_2 begins at temperature below 180˚C, and Fe is obtained at temperature in a range of 500 - 700˚C in Ar or N_2 flow [120-123].

Iron carbides, Fe_3C (cementite) for instance, are most stable in the temperature range from 600 ˚C to 750˚C. At temperature above 750˚C, the thermal decomposition of cementite increases with an increase in temperature and small iron particles and C are generated [124]. This decomposition process in metal carbides is called metal dusting [125-127]. Since metal carbonitrides, nitrides, and carbides seem to be unstable at 1000˚C, it is speculated that γ–$(Fe, Si)_x$ (siliside = silica-containing austenite) and $(Fe,Ni,Si)_x$ (iron–nickel silicides = silica-containing binary alloy) are formed together with C and N_2 by the metal dusting, as shown below.

$$(Fe,Si)_x(C,N)_{1-y} \rightarrow \gamma - (Fe, Si)_x + C_{1-y} + 0.5N_{2(1-y)} \ (< 700^{\circ}C)$$ [114]

$$(Fe,Ni,Si)_x(C,N)_{1-y} \rightarrow (Fe,Ni,Si)_x + C_{1-y} + 0.5N_{2(1-y)}$$

5. 1. 7 Recarburization and/or nitrocarburization

There are papers suggesting the presence of alloyed α–$(Fe,Si)_x$ (siliside) and $(Fe,Si)_xC$ in CNTs, indicated by EDX after the CCVD reaction at 750˚C and 900˚C [112-114]. These papers imply that most of CNTs start to grow from α–$(Fe,Si)_x$, not from $(Fe,Si)_xC$. Thus, after the metal dusting, alloyed γ–$(Fe,Si)_x$ and $(Fe,Ni,Si)_x$ may be again carburized and/or nitrocarburidized to form $(Fe,Si)_xC_y$ and $(Fe,Ni,Si)_xC_y$, as follows.

$$\gamma - (Fe,Si)_x + C \rightarrow (Fe,Si)_xC_y \ (900^{\circ}C)$$ [117,118]

$$(Fe,Ni,Si)_x + C \rightarrow (Fe,Ni,Si)_xC_y$$

5. 1. 8 Liberation and/or ionization

Finally, Si might be liberated due to its extremely higher ionization energy compared to that of C. As previously mentioned, these metal carbides are less reactive

compared to γ–$(Fe,Si)_x$ and $(Fe,Ni,Si)_x$ and are thermally unstable.

$(Fe,Si)_xC_y \rightarrow Fe_xC_y + Si_x$ (900˚C) [117,118]

$(Fe,Ni,Si)_xC_y \rightarrow (Fe,Ni)_xC_y + Si_x$

In another insight, when the flux of C is very large, the metal dusting process may slow down or not be sufficiently completed. This may also lead to Fe_xC_y and $(Fe,Ni)_xC_y$ remaining as is after nitrocarburization and being included in CNTs.

These steps of changes in the catalyst structure during the oxidation followed by the growth of CNTs are schematically illustrated in Figure 33.

[Step 1]

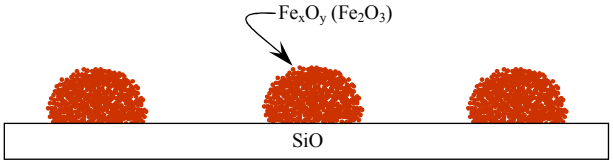

- Impregnation of metal oxides to SiO
- Synthesis of Iron oxides : e.g. α/γ-Fe_2O_3

[Step 2]

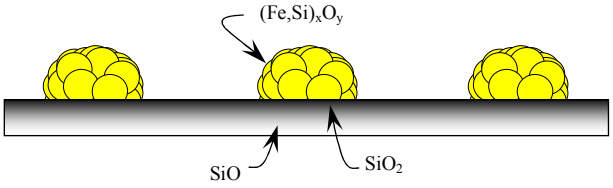

- Si including metal oxides :
  $SiO + Fe_xO_y \rightarrow SiO_2 + Si + (Fe,Si)_xO_y$

[Step 3]

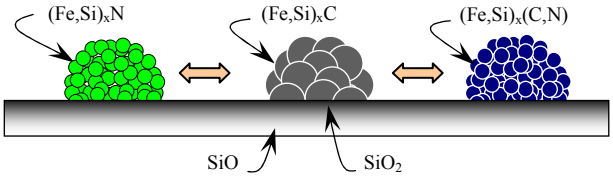

- NH_3 decomposition : $NH_3 \rightarrow 0.5N_2 + 1.5H_2$
- CH_4 decomposition : $CH_4 \rightarrow C + 2H_2$
- Nitrocarburization : $(Fe,Si)_xO_y + C + N_2 \rightarrow (Fe,Si)_x(C,N)_y$

[Step 4]

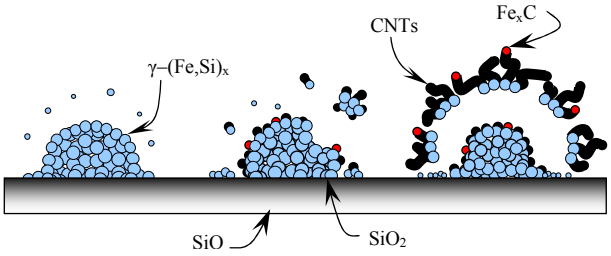

- Denitrocarburization (Metal dusting) :
  $(Fe,Si)_x(C,N)_y \rightarrow \gamma$–$(Fe,Si)_x + C + N_2$
- Refinement of Silisides ;
  γ–$(Fe,Si)_x \rightarrow$ Catalytic aerosol siliside
- Recarburization ;
  Silisides γ–$(Fe,Si)_x + C \rightarrow Fe_xC + Si$

[Step 5]

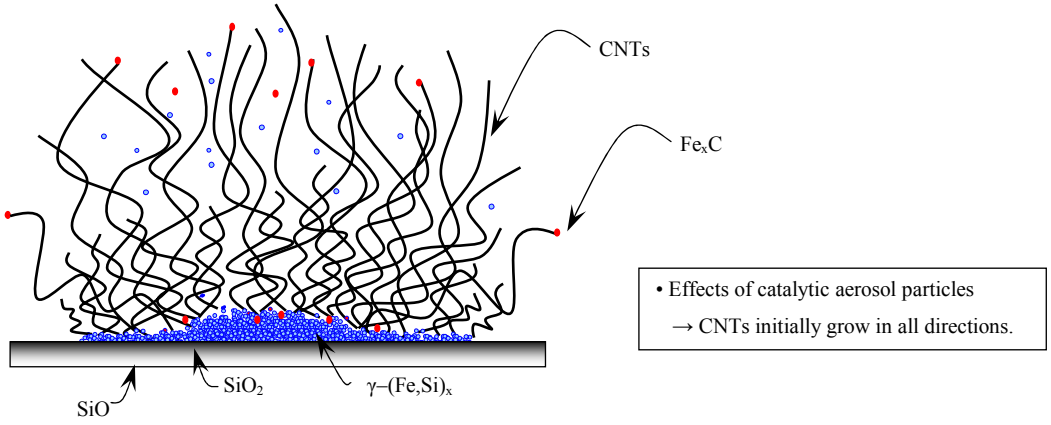

[Step 6]

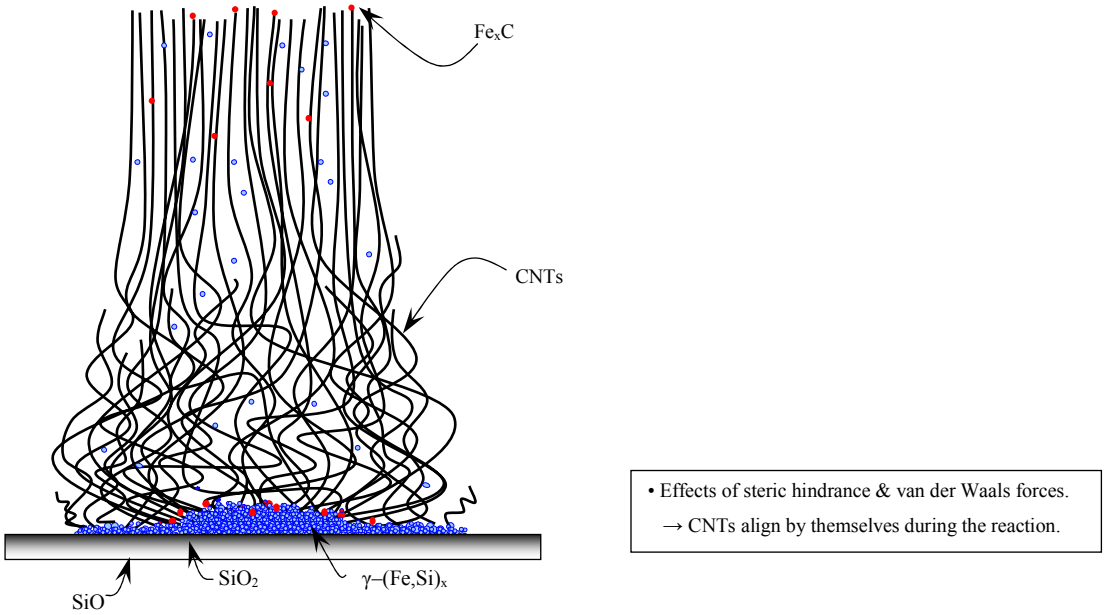

Figure 33. Schematic illustration of a possible CNT growth mechanism

5. 2 Effects of SiO particle size

The differences derived from SiO of two different particle sizes seem to be attributed to the difference of the surface area of SiO. In general, the smaller the size of particles, the larger the surface area per mass of particles. It would be easier to distribute metal clusters over a large surface than over a small surface. The results described in Section 4. 1 are very complex and do not follow this general trend. There might be differences resulting from the sources of SiO particles used. In addition, relationships between the surface area of SiO and catalyst activity, and how they affect the growth of CNTs, are also unknown. Further study is needed.

5. 3 Effects of metal composition

Iron oxides (Fe_xO_y) and nickel oxides ($Ni_{1-x}O$) have possibilities to form metal deficient crystal structures. Larger metal deficient crystal structures generate larger mobility of ions due to creation of vacancies and enhance the reactivity of metal oxides. Since the range of non-stoichiometry in $Ni_{1-x}O$ is very narrow compared to that in Fe_xO_y, namely $Fe_{1-x}O$ [128], the crystal structure of $Ni_{1-x}O$ might be more stable than that of Fe_{1-x} O. It is speculated that the instability of crystal structure may be one of the factors relevant to the higher catalytic activity of iron oxides.

It is suggested to load Fe at a fraction of approximately 70% or higher in order to achieve high CNT yields. However, differences in properties of product CNTs grown from single metal catalysts or bimetallic catalysts are known yet. Further study is needed.

5. 4 Effects of metal loading

Transitional metals, such as Fe and Ni, have strong dipole-dipole interactions, and it is suggested that they tend to easily aggregate each other and to form larger clusters. An increase in the metal loading may enhance aggregation of metal clusters. However, any facts between their aggregation and the growth of CNTs were not developed in this study. Further study is necessary.

5. 5 Effects of catalyst oxidation temperature

In the range of temperature used for oxidation of catalysts in this study, it is expected that nano-sized hematite (α–Fe_2O_3) clusters or maghemite (γ–Fe_2O_3) clusters are formed [128-131]. Comparing the crystal structures of these single metallic oxides, one may notice that α–Fe_2O_3 is the most stable iron oxide due to its corundum crystal structure while γ–Fe_2O_3 has the defect-spinel-type crystal structure, represented as $(Fe^{III})_A(\square_{1/3}Fe^{III}_{5/3})_BO_4$, where $\square$ represents a vacancy, A and B indicate tetrahedral and octahedral sites, respectively. Since such defective structures are associated with the activity of metals, the temperature at which γ–Fe_2O_3 is formed will be favored for the CNT growth, which is in the range from 450°C to 650°C [107, 130]. Furthermore, since γ–Fe_2O_3 exists paramagnetically above the Neel temperature, 600°C, it is suggested that temperature from 600°C to 650°C may be adequate for oxidation of Fe-based catalysts.

As mentioned in Section 5. 3, in Fe-Ni bimetallic oxides, both iron and nickel oxides may be of metal deficient crystal structures, and nickel oxides will be more

stable. In order to activate nickel oxides, defect concentrations need to be increased, followed by a decrease in the Gibbs free energy. The temperature at which the Gibbs free energy becomes minimum for Fe-Ni bimetallic oxides seems to be higher than single Fe metallic oxides, and this may explain the fact that Fe-Ni bimetallic catalysts are more active when they are oxidized at higher temperature.

It is implied from SEM observations that nucleation of metals and their agglomeration are enhanced at higher temperature. These seem to be one of the factors causing the formation of nanotubes of larger sizes. On the other hand, crucial effects are not clear. Other methods for detailed analysis are needed to specify real effects.

5. 6 Effects of catalysts grinding

There are some reports regarding influences of grinding on catalytic properties. One of the studies indicates that an increase in the grinding time enhances activity of catalysts due to an increase in the degree of lattice disorder [132]. When there are solid phases more than two, such as Fe, $Fe_{1-x}O$, and Fe_xO_y, after oxidizing SiO supported catalysts, simple manual grinding may strongly affect electron mobility from the metal oxides to the reaction medium [110, 133, 134]. Another study also suggests that grinding is necessary for forming active catalysts, because it affects interactions between metal oxides leading to an increase in the interface area [135]. Thus, it is speculated that the lattice disorder derived from grinding enhances catalyst activity, affecting the ability of electron transfer and interaction in catalysts, and

eventually promotes the CNT growth. In order to analyze effects of grinding, further study is needed.

5. 7 Effects of NH_3 pretreatment

It is obvious that the sublimation of SiO is extremely small at the reaction temperature in the range investigated in this research, even though transition metals are impregnated onto SiO (see Appendix D). It is indicated in Figures 23 and 24 that the particle sizes of SiO tend to decrease with an increase in the time for the NH_3 pretreatment. Furthermore, it is also suggested, in Figures 25 and 26, that NH_3 strongly affects the surface morphology of catalysts. As already discussed, N_2 generated from the thermal decomposition of NH_3 acts as a strong reducing agent and rapidly replaces O_2 in metal oxides. In addition, it is reported that this activated N_2 has strong power to open up the lattice in *bcc* α−Fe and to convert it to the *fcc* lattice [117]. Hence, the refinement in catalytic metal particles derived from nitridation may be related to the effects of pretreatment.

An increase in the pretreatment will forward nitridation of metal oxides. This may prevent the liberation of N_2 that could be necessary for the formation of more active metal catalysts, such as siliside, influencing the CNT growth. Further study is needed.

5. 8 Reaction temperature effects

The growth rate of CNTs increases with an increase in the reaction temperature. However, at temperature above 1000°C, it decreases with a further increase in the reaction temperature. The decrease in the CNT growth rate is considered to be associated with deactivation of catalysts. An increase in the formation of metal carbides or metal carbonitrides with temperature, which are less active than silicides, is speculated. In addition, since the diffusivity of SiO will be promoted with an increase in temperature, this may also affect the growth of CNTs. Further investigations are necessary to clarify conclusive effects.

5. 9 Dependencies on reaction time

It is suggested that two phenomena, deactivation of catalysts and a limit to the diffusion of C derived from CH_4 are associated with the growth termination of CNTs. The following assumptions may be made as a possible mechanism: catalytic silicides may react with C to form carbides due to a gradual loss of Si, and this may lead to a limit of the activity of catalysts [113, 114], and the limit to gas diffusion is attributed to the thickening mat of CNTs surrounding metal catalysts [56]. It may be also considered that an increase in the thickness of CNT walls decreases the surface energy and elastic energy of metal catalysts. Hence, the growth may be eventually terminated.

5. 10 Effects of NH_3/CH_4 feed ratio

Figure 32 may imply that an increase in the NH_3 feed affects the formation of silicides and their activity due to supply of an excess N_2 derived from NH_3. Nitridation and carburization can occur at the same time, and N_2 has stronger effects on these reactions than C. As the concentration of N_2 increases in metal oxides, the liberation of N_2 or decomposition of metal carbides (called the metal dusting [125−127]) may become slow. Thus, the reaction rate to form silicides may also decrease. Furthermore, it is considered that an excess amount of NH_3 may cause the formation of metal carbonitirdes after silicides are generated and then decrease the growth rate of CNTs. In addition, a decrease in the CH_4 concentration with an increase in the NH_3/CH_4 ratio would also affect the CNT growth. Further study is necessary.

6. CONCLUSION

6. 1 Summary

CNTs were successfully synthesized on SiO supports using Fe and Fe−Ni bimetallic catalysts via the catalytic CVD from NH_3/CH_4 mixtures. The effects on the growth of CNTs of SiO particle size, metal composition, metal loading, catalyst oxidation temperature, grinding of catalysts, NH_3 pretreatment time, reaction temperature, reaction time, and NH_3/CH_4 feed ratio, were investigated.

Catalysts supported on 44 μm average-sized SiO particles gave higher yields of CNTs than those on 8 μm average-sized SiO particles, when no NH_3 pretreatment was performed. Catalysts containing 1 wt% Fe/SiO produced aligned CNTs and yielded higher growth rates per mass of metal than Fe-Ni bimetallic catalysts. Temperature between 600°C and 750°C was found to be optimum for oxidizing 1 wt% Fe-loaded catalysts while a range of 450 - 600°C was proper for the oxidation of 3 wt% Fe, and 750 - 900°C for Fe-Ni bimetallic catalysts, to achieve high yields of CNTs. Grinding catalysts for 3 minutes or longer increased the CNT growth rate. The yield of CNTs decreased with an increase in the NH_3 pretreatment time, regardless of metal compositions. However, CNTs did not grow appreciably from methane without ammonia. An NH_3/CH_4 feed ratio of 0.15 - 0.25 was observed to give highest yields of CNTs. The optimum reaction temperature for the CNT growth was found to lie in the range between 990°C and 1000 °C. The growth rate decreased with reaction time.

Table 9 summarizes the results obtained in this study. These results could be used as optimum conditions for producing CNTs on Fe or Fe-Ni catalysts, when SiO

is used as the metal supporting substrate.

Table 9. Summary of results obtained in this research

Process	Parameters	Results (Max. CNTs growth rate)
Catalyst	Support (SiO) particle size	40 μm D > 8 μm D.* (* : no NH_3 pretreatment)
	Transition metal activity	Fe > Fe-Ni
	Composition (metal/SiO)	Fe : 1 wt% Fe is best. Fe-Ni : 2 wt% Fe - 1 wt.% Ni is best.
Oxidation	Temperature	600 - 750°C (1 wt% Fe) 450 - 600°C (3 wt% Fe) 750 - 900°C (2 wt% Fe - 1 wt% Ni)
Grinding	Time	a minimum of 3 min
Pretreatment	Time	No pretreatment.
Reaction	Temperature	990 - 1000°C (3 wt% Fe) 990 - 1000°C (2 wt% Fe - 1 wt% Ni)
	NH_3/CH_4 feed Ratio	0.15 - 0.25 (3 wt% Fe)

6. 2 Recommendations for future work

After impregnation of metals onto SiO, followed by oxidation, it is suspected that iron oxides containing Si are synthesized. The activity of catalysts will be different depending on iron oxides. In this method, there still seem to be possibilities to improve the activity by reduction or some other chemical/physical treatments. It is recommended to characterize metals synthesized and surface properties of supporting substrates using such methods as Energy Dispersive X-ray (EDX) analysis and X-ray Diffraction (XRD) analysis. Applying molecular dynamic and energy functions may reveal important limiting factors, such as electron mobility.

Through this study, most of quantitative investigations regarding influences of process parameters were made. However, observations of product quality were not carried out intensively. It is advised to know the growth mechanism and significant factors for controlling the product quality using appropriate characterization methods and analytical tools. Furthermore, an appropriate type of reactor and its suitable material should be selected based on kinetic study. Production efficiencies will need to be analyzed, considering product quality, in order for practical applications of this process to be realized.

BIBLIOGRAPHY

1. H. W. Krote, J. R. Heath, S. C. O'Brien, R. F. Curl, and R. E. Smalley, *Nature*, **318**, 162(1985)

2. S. Iijima, *Nature*, **354**, 56(1991)

3. X. Zhao, T. Kadoya, T. Ikeda, T. Suzuki, S. Inoue, M. Ohkohchi, Y. Takimoto, and Y. Ando, *Diamond and Related Materials*, **16**, 1101(2007)

4. M. Cadek, R. Murphy, B. McCarthy, A. Drury, B. Lahr, R. C. Barklie, M. in het Panhuis, J. N. Coleman, and W. J. Blau, *Carbon*, **40**, 923(2002)

5. I. A. Kinloch, G. Z. Chen, J. Howes, C. Boothroyd, C. Singh, D. J. Fray, and A. H. Windle, *Carbon*, **41**, 1127(2003)

6. I.A. Novoselova, N.F. Oliinyk, S.V. Volkov, A.A. Konchits, I.B. Yanchuk, V.S. Yefanov, S.P. Kolesnik, and M.V. Karpets, *Physica E: Low-dimensional Systems and Nanostructures*, **40**, 2231(2008)

7. F. Wei, Q. Zhang, W. Z. Qian, H. Yu, Y. Wang, G. H. Luo, G. H. Xu, and D. Z. Wang, *Powder Technology*, **183**, 10(2008)

8. Y. Wang, F. Wei, G. Luo, H. Yu, and G. Gu, *Chemical Physics Letters*, **364**, 568(2002)

9. S. Kimura and K. Williamson, "Methods for Fabricating Individual Nanotubes," *U.S. patent application*, October, 2006.

10. Y. F. Zhang, Y. H. Tang, C. Lam, N. Wang, C. S. Lee, I. Bello, and S. T. Lee, *Journal of Crystal Growth*, **212**, 115(2000)

11. B. Pivac, P. Dubček, I. Capan, H. Zorc, S. Bernstorff, S. Duguay, and A. Slaoui, *Thin Solid Films*, Available online, Dec.8, 2007

12. A. J. Nuth and F.T Ferguson, *Astrophysical Journal*, **649**, 1178(2006)

13. X. H. Fan, L. Xu, C. P. Li, Y. F. Zheng, C. S. Lee, and S. T. Lee, *Chemical Physics Letters*, **334**, 229(2001)

14. Z. Jianfeng, H. Min, L. Minda, S. Fengqi, W. Jianguo, C. Yanfeng, and W. Guanghou, *Journal of Crystal Growth*, **269**, 207(2004)

15. Y. Takakuwa, M. Nihei, N. Miyamoto, *Applied Surface Science*, **117**, 141 (1997)

16. R. Tromp, G. W. Rubloff, P. Balk, and F. K. LeGoues, *Physical Review Letters*, **55**, 2332(1985)

17. E. A. Rohlfing, D. M. Cox, A. Kaldor, *The Journal of Chemical Physics*, **81**, 3322(1984)

18. http://www.jcrystal.com/steffenweber/gallery/Fullerenes/Fullerenes.html

19. http://www.physorg.com/news98026698.html, Shanov, M. Schulz, University of \Cincinnati, "The longest carbon nanotubes you've ever seen"

20. http://physicsworld. Com/cws/article/print/1761,

21. http://www.nanotech-now.com/nanotube-buckyball-sites.htm

22. http://dictionary.zdnet.com/definition/Nanotube.html

23. H. Dai, *Surface Science*, **500**, 218(2002)

24. R. Saito, *Kagaku*, 68(1998)

25. R. Saito, M. Fujita, and G. Dresselhaus, *Applied Physics Letters*, **60**, 2204 (1992)

26. A. P. Ramirez, *Bell Labs Technical Journal*, **10**(3), 171(2005)

27. L. E. Foster, *Nano Technology,* Prentice Hall, 2006

28. K. T. Kashyap, R. G. Patil, *Bulletin of Materials Science*, **31**, 185(2008)

29. O. Lourie, H. D. Wagner, *Journal of Materials Research*, **13**, 2418(1998)

30. S. Niyogi, M. A. Hamon, H. Hu, B. Zhao, P. Bhowmik, R. Sen, M. E. Itkis, R. C. Haddon, *Accounts of chemical Research*, **35**, 1105(2002)

31. J. Giraudet, M. Dubois, D. Claves, J. P. Pinheiro, M. C. Schouler, P. Gadelle, A. Hamwi, *Chemical Physics Letters*, **381**, 306(2003)

32. C. Zhao, L. Ji, H. Liu, G. Hu, S. Zhang, M. Yang, Z. Yang, *Journal of Solid State Chemistry*, **177**, 4394(2004)

33. Y. Tsukahara, T. Yamauchi, T. Kawamoto, Y. Wada, *J. Chemical Society of Japan*, **81**, 387(2008)

34. M. Damnjanović [*], I. Milošević, T. Vuković, and R. Sredanović, *Physical Review B*, **60**, 2728(1999)

35. A.B. Dalton, H.J. Byrne, J.N. Coleman, S. Curran, A.P. Davey, B. McCarthy, and W. Blau, *Synthetic Metals*, **102**, 1176(1999)

36. Z. Jin, L. Huang, S. H. Goh, G. Xu. W. Ji, *Chemical Physics Letters*, **352**, 328(2002)

37. Q. Wang, Y. Qin, Y. Zhu, X. Huang, Y. Tian, P. Zhang, Z. Guo, Y. Wang, *Chemical Physics Letters*, **457**, 159(2008)

38. A. B. Dalton, J. N. Coleman, M. I. H. Panhuis, B. McCarthy, A. Drury, W. J. Blau, B. Paci, J. M. Nunzi, and H. J. Byrne, *Journal of Photochemistry and Photobiology A: Chemistry*, **144**, 31(2001)

39. M. Paradise and T. Goswami, *Materials & Design*, **28**, 1477(2007)

40. A. P. Graham, G. S. Duesberg, R. Seidel, M. Liebau, E. Unger, F. Kreupl, and W. Hönlein, *Diamond and Related Materials*, **13**, 1296(2004)

41. http://www.azonano.com/details.asp, Applications of Carbon Nanotubes (Buckytubes)

42. D. S. Bethune, C.-H. Kiang, M. S. de Vries, G. Gorman, R. Savoy, J. Vazquez, and R. Beyers, *Nature*, **363**, 605(1993)

43. P. J.F. Harris, *Carbon*, **45**, 229(2007)

44. T. Guo, P. Nikolaev, A. Thess, D.T. Colbert, and R.E. Smalley, *Chemical Physics Letters*, **243**, 49(1995)

45. T. Guo, P. Nikolaev, A. G. Rinzler, D. Tomanek, D. T. Colbert, and R. E. Smalley, *Journal of Physical Chemistry*, **99**, 10694(1995)

46. Y. Saito, *Carbon*, **33**, 979(1995)

47. D. Nishide, H. Kataura, S. Suzuki, K. Tsukagoshi, Y. Aoyagi, and Y. Achiba, *Chemical Physics Letters*, **372**, 45(2003)

48. O. Smiljanic, B. L. Stansfield, J. -P. Dodelet, A. Serventi, and S. Désilets *Chemical Physics Letters*, **35**6, 189(2002)

49. K. B. Shelimov, R. O. Esenaliev, A. G. Rinzler, C. B. Huffman, and R. E. Smalley, *Chemical Physics Letters*, **282**, 429(1998)

50. E. Mizoguti, F. Nihey, M. Yudasaka, S. Iijima, T. Ichihashi, and K. Nakamura *Chemical Physics Letters*, **321**, 297(2000)

51. M. Zhang, M. Yudasaka, and S. Iijima, *Chemical Physics Letters*, **336**, 196(2001)

52. S. Costa, C. Tripisciano, E. Borowiak-Palen, and R.J. Kalenczuk, *Energy Conversion and Management*, Available online, May 9, 2008

53. B.I. Yakobson, and R.E. Smalley, *American Scientist*, *85*, 324(1997)

54. M. Jose-Yacaman, M. Miki-Yoshida, and L. Rendon, *Applied Physics Letter*, **62**, 657(1993)

55. J. Kong, A. M. Cassell, and H. Dai, *Chemical Physics Letters*, **292**, 567(1998)

56. A. M. Cassell, J. A. Raymakers, J. Kong, and H. Dai, *The Journal of Physical Chemistry B*, **103**, 6484(1999)

57. J. H. Hafner, M. J. Bronikowski, B. R. Azamian, P. Nikolaev, A. G. Rinzler, D. T. Colbert, K. A. Smith, and R. E. Smalley, *Chemical Physics Letters*, **296**, 195(1998)

58. Z. H. Yuan, H. Huang, L. Liu, and S. S. Fan, *Chemical Physics Letters*, **345**, 39(2001)

59. K. Y. Tran, B. Heinrichs, J. F. Colomer, J. P. Pirard, and S. Lambert, *Applied Catalysis A*, **318**, 63(2007)

60. H. M. Cheng, F. Li, X. Sun, S. D. M. Brown, M. A. Pimenta, A. Marucci, G. Dresselhaus, and M. S. Dresselhaus, *Chemical Physics Letters*, **289**, 602(1998)

61. M. Mayne, N. Grobert, M. Terrones, R. Kamalakaran, M. Rühle, H. W. Kroto, and D. R. M. Walton, *Chemical Physics Letters*, **338**, 101(2001)

62. Y. Tian, Z. Hu, Y. Yang, X. Chen, W. Ji, and Y. Chen, *Chemical Physics Letters*, **388**, 259(2004)

63. E. Couteau, K. Hernadi, J. W. Seo, L. Thiên-Nga, Cs. Mikó, R. Gaál, and L. Forró, *Chemical Physics Letters*, **378**, 9(2003)

64. A. Hamwi, H. Alvergnat, S. Bonnamy, and F. Béguin, *Carbon,* **35**, 723(1997)

65. H. Dai, A. G. Rinzler, P. Nikolaev, A. Thess, D. T. Colbert, and R. E. Smalley, *Chemical Physics Letters*, **260**, 471(1996)

66. P. Nikolaev, M. J. Bronikowski, R. K. Bradley, F. Rohmund, D. T. Colbert, K. A. Smith, R. E. Smalley, *Chemical Physics Letters*, **313**, 91(1999)

67. Y. H. Tang, Y. F. Zheng, C. S. Lee, N. Wang, S. T. Lee, and T. K. Sham, *Chemical Physics Letters*, **342**, 259(2001)

68. A. Fonseca, K. Hernadi, J. B. Nagy, D. Bernaerts, and A. A. Lucas, *Journal of Molecular Catalysis A: Chemical*, **107**, 159(1996)

69. Z. Y. Juang, I. P. Chien, J. F. Lai, T. S. Lai, and C. H. Tsai, *Diamond and Related Materials*, **13**, 1203(2004)

70. C. M. Chen, Y. M. Dai, J. G. Huang, and J. M. Jehng, *Carbon*, **44**, 1808(2006)

71. M. Chen, C. M. Chen, and C. F. Chen, *Journal of Materials Science*, **37**, 3561 (2002)

72. Z. Huang, D. Z. Wang, J. G. Wen, M. Sennett, H. Gibson, and Z. F. Ren, *Applied Physics A – Materials Science & Processing*, **74**, 387(2002)

73. M. Su, B. Zheng, and J. Liu, *Chemical Physics Letters*, **322**, 321(2000)

74. B. Zheng, Y. Li, and J. Liu, *Applied Physics A: Materials Science & Processing*, **74**, 387(2002)

75. P. Nikolaev, M. J. Bronikowski, R. K. Bradley, F. Rohmund, D. T. Colbert, K. A. Smith, and R. E. Smalley, *Chemical Physics Letters*, **313**, 91(1999)

76. R. E. Smalley and B. I. Yakobson, *Solid State Communications*, **107**, 597(1998)

77. K.B. Kouravelou, S.V. Sotirchos, and X.E. Verykios, *Surface and Coatings Technology*, **201**, 9226(2007)

78. R. Alexandrescu, A. Crunteanu, R. E. Morjan, L. Morjan, F. Rohmund, L. K. L.Falk, G. Ledoux, and F. Huisken, *Infrared Physics & Technology*, **44**, 43(2003)

79. D.E. Resasco, W.E. Alvarez, F. Pompeo, L. Balzano, J.E. Herrera, B. Kitiyanan, and A. Borgna, *Journal of Nanoparticle Research*, **4**, 131(2002)

80. http://www.ou.edu/engineering/nanotube/comocat.html

81. C. J. Lee, S. C. Lyu, H. W. Kim, C. Y. Park, and C. W. Yang, *Chemical Physics Letters*, **359**, 109(2002)

82. http://engineering.tamu.edu/safety/guidelines/Nanotechnology/Wondrous

83. M. Su, B. Zheng, and J. Liu, *Chemical Physics Letters*, **322**, 321(2000)

84. Y. Ouyang, L. Chen, Q.X. Liu, and Y. Fang, *Spectrochimica Acta Part A: Molecular and Biomolecular Spectroscopy*, Available online, 2007

85. S. G. Kang, K. K. Cho, K. W. Kim, and G. B. Cho, *Journal of Alloys and Compounds*, **449**, 269(2008)

86. X. Devaux and M. Vergnat, *Physica E: Low-dimensional Systems and Nanostructures*, **40**, 2268(2008)

87. H. Ichioka, N. Higashi, Y. Yamada, T. Miyake, and T. Suzuki, *Diamond and Related Materials*, **16**, 1121(2007)

88. M. Pérez-Mendoza, C. Vallés, W.K. Maser, M.T. Martínez, S. Langlois, J.L. Sauvajol, and A.M. Benito, *Carbon*, **43**, 3034(2005)

89. J. M. Xu, X. B. Zhang, Y. Li, X. Y. Tao, F. Chen, T. Li, Y. Bao, and H. J. Geise, *Diamond and Related Materials*, **13**, 1807(2004)

90. H. Li, C. Shi, X. Du, C. He, J. Li, and N. Zhao, *Materials Letters*, **62**, 1472(2008)

91. H. Li, N. Zhao, C. He, C. Shi, X. Du, and J. Li, *Materials Science and Engineering: A*, **473**, 355(2008)

92. N. Zhao, C. He, Z. Jiang, J. Li, and Y. Li, *Materials Letters*, **60**, 159(2006)

93. K. Hernadi, A. Fonseca, J.B. Nagy, D. Bernaerts, J. Riga, and A. Lucas, *Synthetic Metals*, **77**, 31(1996)

94. E. Flahaut, A. Peigney, Ch. Laurent, and A. Rousset, *Journal of Materials Chemistry*, **10**, 249(2000)

95. J. F. Colomer, P. Piedigrosso, A. Fonseca, and J. B. Nagy, *Synthetic Metals*, **103**, 2482(1999)

96. E. Salernitano, L. Giorgi, Th. Dikonimos Makris, R. Giorgi, N. Lisi, V. Contini, and M. Falconieri, *Diamond and Related Materials*, **16**, 1565(2007)

97. S. Porro, S. Musso, M. Vinante, L. Vanzetti, M. Anderle, F. Trotta, and A. Tagliaferro, *Physica E: Low-dimensional Systems and Nanostructures*, **37**, 58(2007)

98. E. Raymundo-Piñero, T. Cacciaguerra, P. Simon, and F. Béguin, *Chemical PhysicsLetters*, **412**, 184(2005)

99. Y. S. Park, Y. C. Choi, K. S. Kim, D. C. Chung, D. J. Bae, K. H. An, S. C. Lim, X. Y. Zhu, and Y. H. Lee, *Carbon*, **39**, 665(2001)

100. L. Valentini, C. Cantalini, L. Lozzi, S. Picozzi, I. Armentano, J. M. Kenny, and S. Santucci, *Sensors and Actuators B: Chemical*, **100**, 33(2004)

101. I. W. Chiang, B. E. Brinson, A. Y. Huang, P. A. Willis, M. J. Bronikowski, J. L.Margrave, R. E. Smalley, and R. H. Hauge, *Journal of Physical Chemistry*, **105**, 8297(2001)

102. M. Kosaka, T. W. Ebbesen, H. Hiura, and K. Tanigaki, *Chemical Physics Letters*, **233**, 47(1995)

103. R. Andrews, D. Jacques, D. Qian, and E. C. Dickey, *Carbon*, **39**, 1681(2001)

104. C. M. Chen, M. Chen, Y. W. Peng, H. W. Yu, and C. F. Chen, *Thin Solid Films*, **498**, 202(2006)

105. M. Chen, H. W. Yu, J. H. Chen, and H. S. Koo, *Diamond and Related Materials*, **16**, 1110(2007)

106. H. Kataura, Y. Kumazawa, Y. Maniwa, Y. Ohtsuka, R. Sen, S. Suzuki, and Y. Achiba *Carbon*, **38**, 1691(2000)

107. K. D. Kim, S. S. Kim, and H. T. Kim, *Journal of Industrial and Engineering Chemistry*, **11**, 584(2005)

108. Y. Li, Z. Y. Luo, C. J. Yu, D. Luo, Z. A. Xu, and K. F. Cen, *Journal of Zhejiang University Science B*, **6**, 1124 (2005)

109. K. Prabhakaran, K. V. P. M. Shafi, A. Ulman, P. M. Ajayan, Y. Homma, and T. Ogino, *Advanced Materials*, **13**, 1859 (2001)

110. Flávia C.C. Moura, Grazielli C. Oliveira, Maria Helena Araujo, José D. Ardisson, Waldemar A.A. Macedo, and Rochel M. Lago, *Applied Catalysis A: General*, **307**, 195(2006)

111. http://www.kobelco.co.jp/technology-review/pdf/55_1/031-036.pdf.

112. Y. Yao, L.K.L. Falk, R.E. Morjan, O.A. Nerushev, and E.E.B. Campbell, *Carbon*, **45**, 2065(2007)

113. Y. Yao, L.K.L. Falk, R.E. Morjan, O.A. Nerushev, and E.E.B. Campbell, *Journal of Materials Science*, **15**, 533(2004)

114. Y. Yao, L.K.L. Falk, R.E. Morjan, O.A. Nerushev, and E.E.B. Campbell, *Journal of Materials Science*, **15**, 583(2004)

115. http://www.caer.uky.edu/caerseminar/shah.shtml

116. http://www.kintecus.com/Kin_05-OLF-CEJC-Dirtu.pdf

117. K. H. Jack, *Proceedings of the Royal Society of London. Series A, Mathematical and Physical Sciences*, **195**, 41(1948)

118. X. Q. Zhao, Y. Liang, Z. Q. Hu, and B. X. Liu, *Journal of Materials Research*, **11**, 2689(1996)

119. C. Jaoul, T. Belmonte, and T. Czerwiec, N. David, *Applied Surface Science*, **252**, 8360(2006)

120. X. Z. Ding, F. M. Zhang, Y. L. Sun, Z. Y. Zhou, X. Wang, X. H. Liu, and D. F. Shen, *Surface and Coatings Technology*, **91**, 215(1997)

121. www.saitama-u.ac.jp/crc/professor/kiyo/h12/19.pdf

122. M. Yamada, Y. Kouzaki, T. Yasui, and M. Fukumoto, *Surface and Coatings Technology*, **201**, 1754(2006)

123. H. Chatbi, M. Vergnat, J. F. Bobo, and L. Hennet, *Solid State Communications*, **102**, 677(1997)

124. J. Zhang, O. Ostrovski, *ISIJ International*, **41**, 333(2001)

125. H. J. Grabke, R. Krajak, and J. C. Nava Paz, *Corrosion Science*, **35**, 141(1993)

126. H. J. Grabke, I. Wolf, *Materials Science and Engineering*, **87**, 23(1987)

127. P. Szakalos, *Materials and Corrosion*, **54**, 752(2003)

128. Shriver & Atkins, "*Inorganic Chemistry*", FREEMAN

129. M. C. Deng, L. H. Chen, M. P. Hung, T. S. Chin, C. H. Lin, *IEEE Transactions on Magnetics*, **25**, 3644(1989)

130. http://www.ritsumei.ac.jp/acd/mr/lib/thesis/abstract/2005/k_359_j.htm

131. B. Tamamushi et al., "*Dictionary of Physics and Chemistry*", Iwanami Bookstore.

132. A. Rougier, S. Soiron, I. Haihal, L. Aymard, B. Taouk, and J. -M. Tarascon, *Powder Technology*, **128**, 139(2002)

133. F.C.C. Moura, M.H. Arau´jo, R.C.C. Costa, W.A.A. Macedo, J.D. Fabris, J.D. Ardisson, and R.M. Lago, *Chemosphere*, **60**, 1118(2005)

134. F.C.C. Moura, M.H. Araujo, G.C. Oliveira, W.A.A. Macedo, J.D. Ardisson, and R.M. Lago, Chemistry Letter, **34**, 1172(2005)

135. Dmitri A. Bulushev, Lioubov Kiwi-Minsker, Vladimir I. Zaikovskii, and Albert Renken, *Journal of Catalysis*, **193**, 145(2000)

APPENDICES

Appendix A; Catalytic Chemical Vapor Deposition (CCVD) System

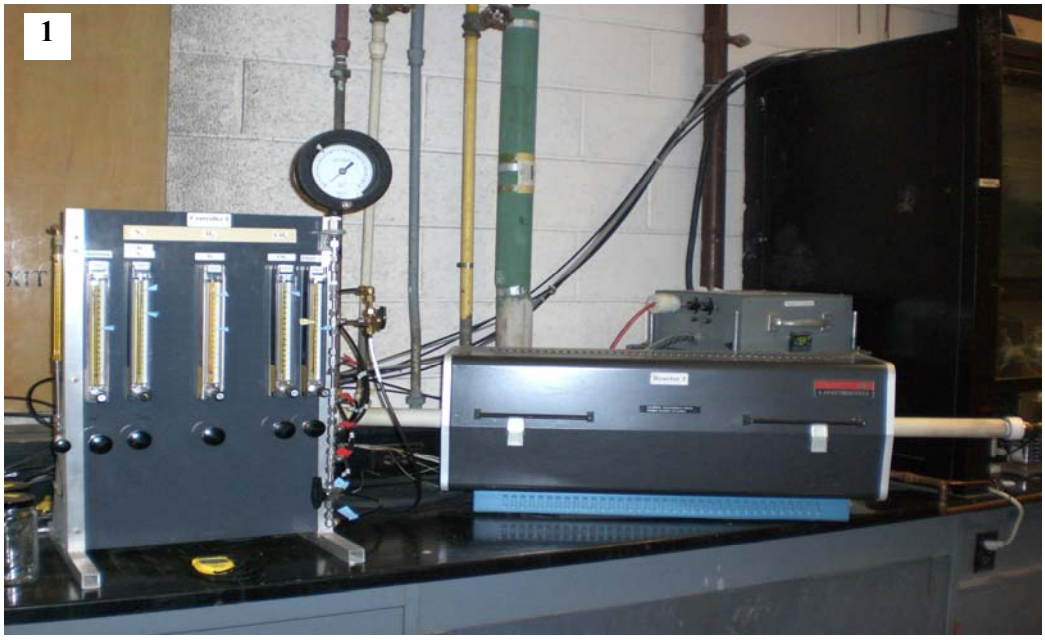

Figure A. 1 CCVD System (controller for the gas feed and a furnace)

Figure A. 2 Furnace

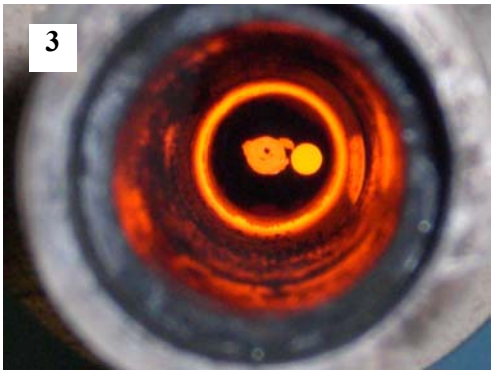

Figure A. 3 Inside of a furnace

Appendix B; Instruments

Figure B. 1 Scanning electron microscope (SEM)

Figure B. 2 Chemical balance

Appendix C; SEM images of CNTs

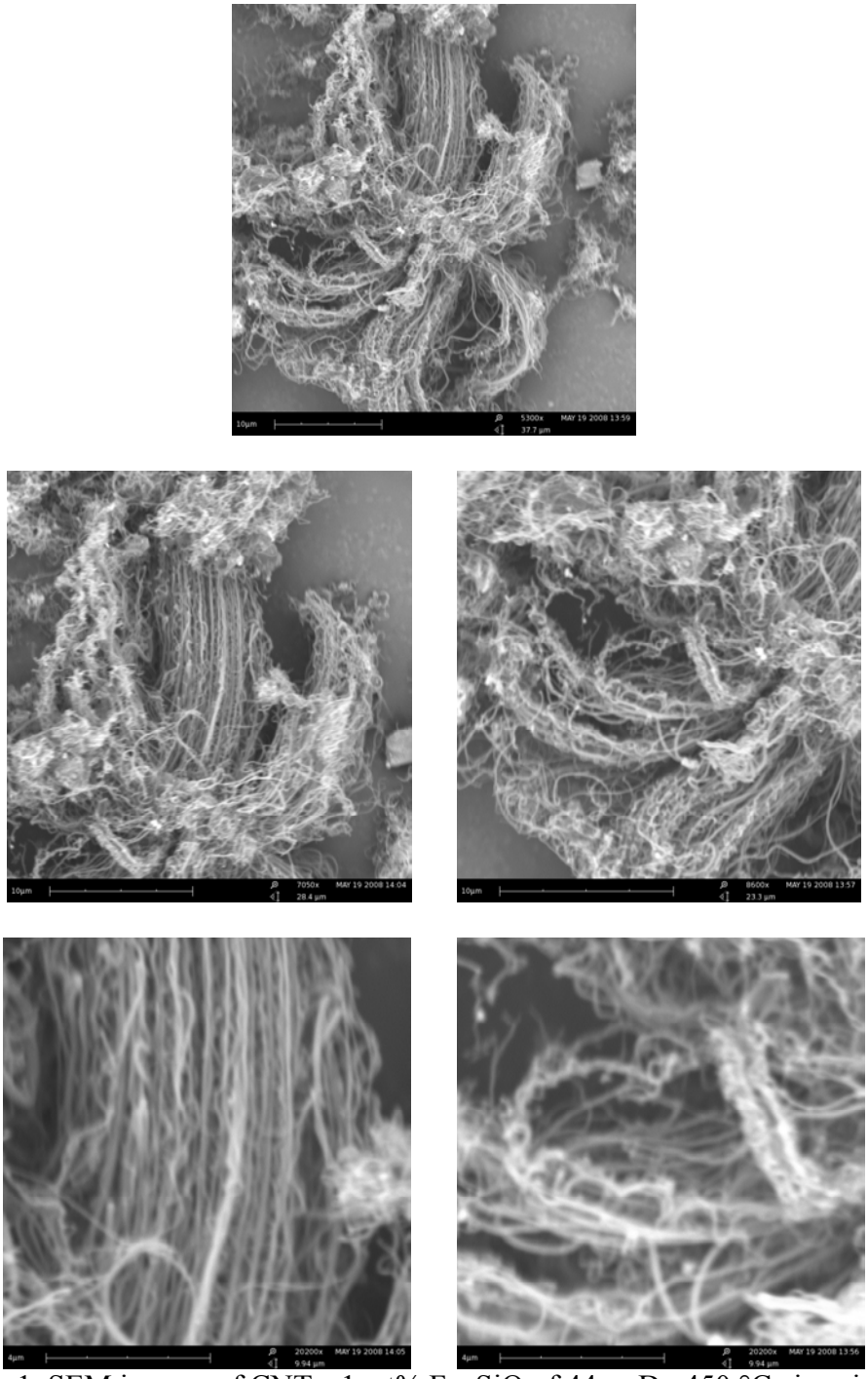

Figure C. 1 SEM images of CNTs; 1 wt% Fe, SiO of 44µmD., 450 °C air oxidation, 1.5 min grinding, No NH_3 pretreatment, 1000°C - 5 min reaction.

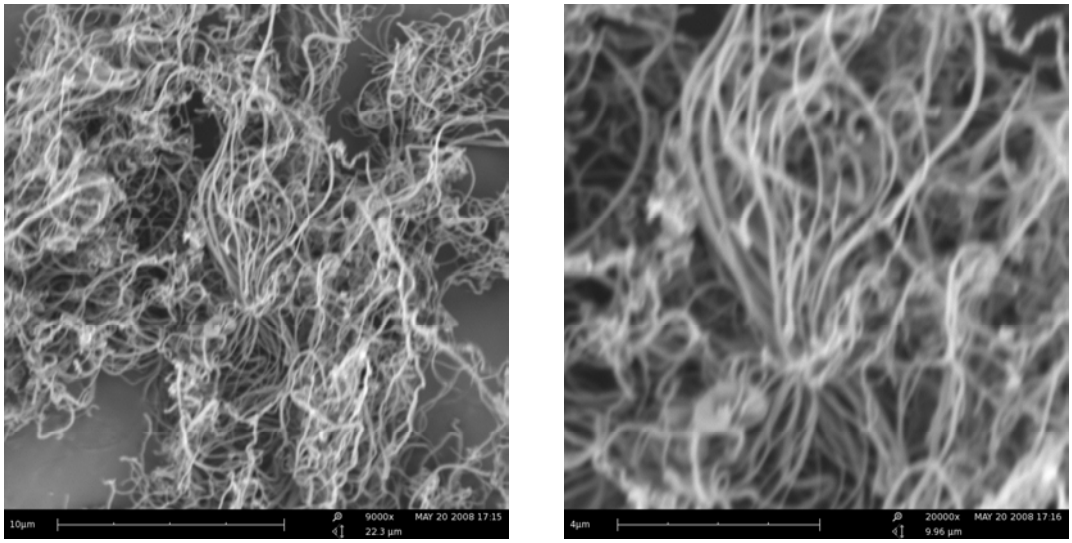

Figure C. 2 SEM images of CNTs; 1 wt% Fe, SiO of 44µmD., 750 °C air oxidation, 1.5 min grinding, No NH_3 pretreatment, 1000°C - 5 min reaction.

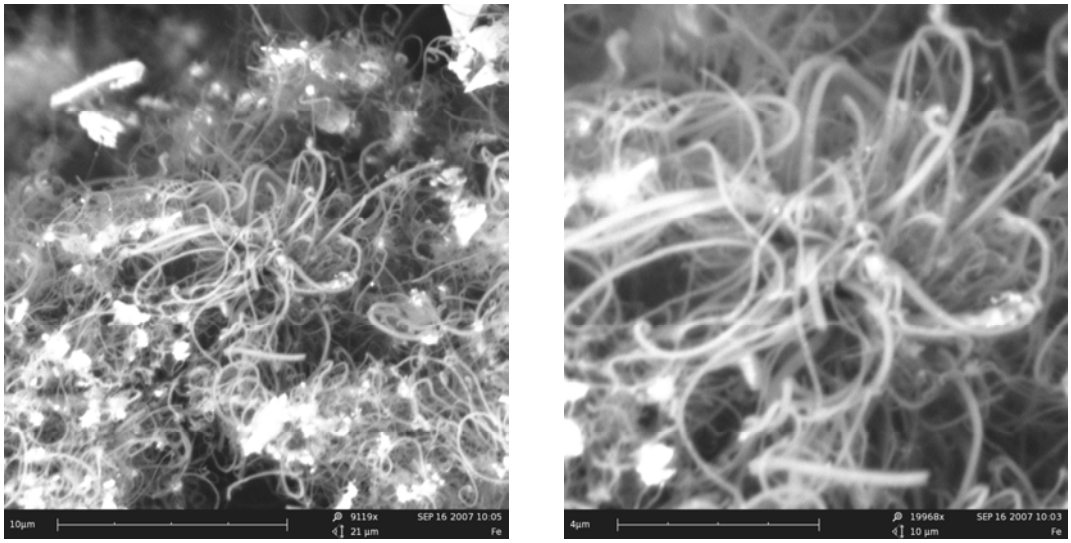

Figure C. 3 SEM images of CNTs; 3 wt% Fe, SiO of 44µmD., 450 °C air oxidation, 1.5 min grinding, No NH_3 pretreatment, 1000°C - 5 min reaction.

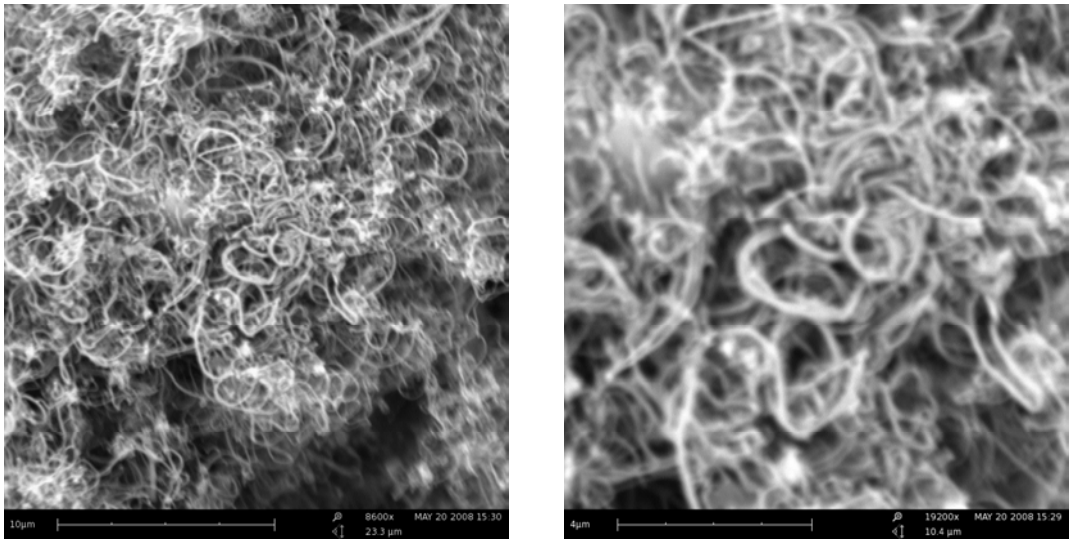

Figure C. 4 SEM images of CNTs; 3 wt% Fe, SiO of 44µmD., 600 °C air oxidation, 1.5 min grinding, No NH_3 pretreatment, 1000°C - 5 min reaction

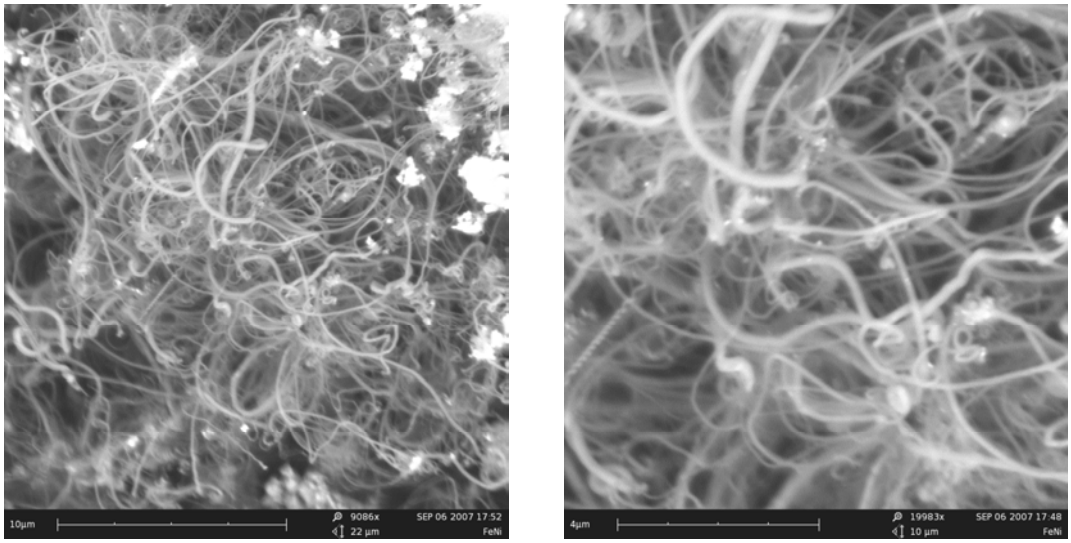

Figure C. 5 SEM images of CNTs; Fe - Ni bimetal (2 wt% Fe - 1 wt% Ni), SiO of 44µmD., 450 °C air oxidation, 1.5 min grinding, No NH_3 pretreatment, 1000°C - 5 min reaction

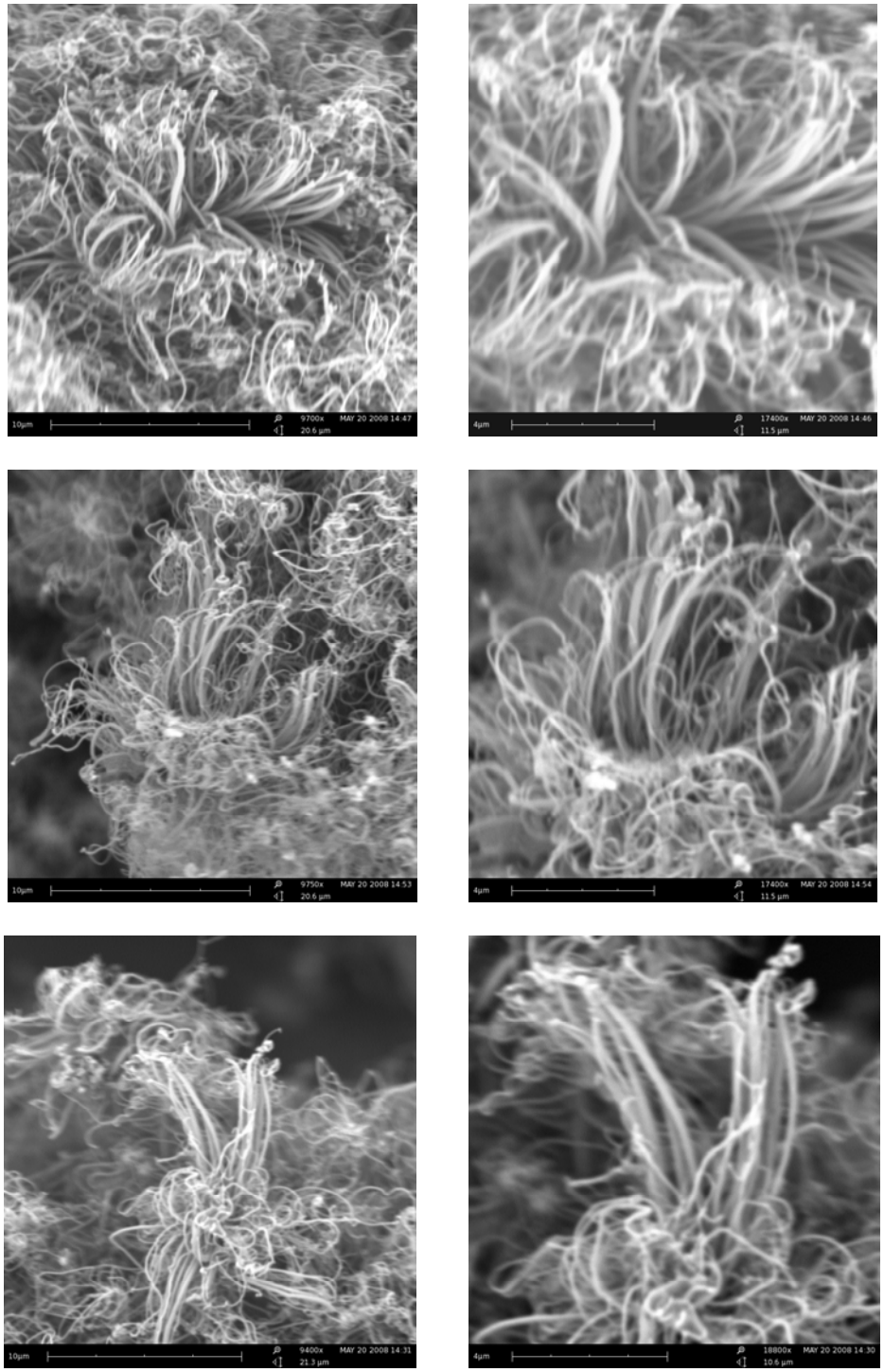

Figure C. 6 SEM images of CNTs; Fe - Ni bimetal (2 wt% Fe - 1 wt% Ni), SiO of 44μmD., 900 °C air oxidation, 1.5 min grind, No NH_3 pretreatment, 1000°C - 5 min reaction.

Appendix D; SiO sublimation rate

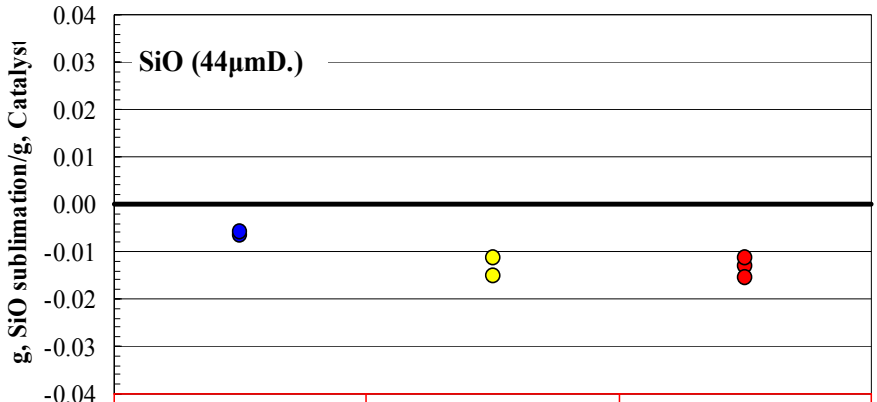

	NH3	N2	Ar
1st run	-0.0067	-0.0152	-0.0132
2nd run	-0.0050	-0.0115	-0.0112
3rd run	-0.0060	-0.0290	-0.0154

Figure D. 1 SiO (44 µm D.) Sublimation rate; 1000°C - 5min

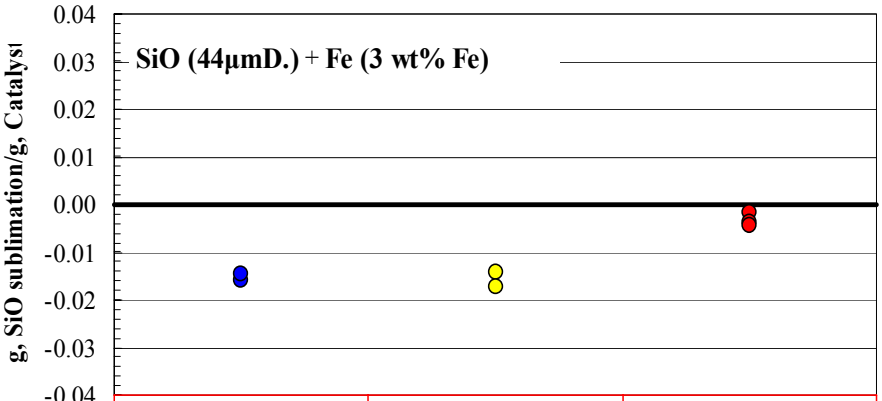

	NH3	N2	Ar
1st run	-0.0158	-0.0141	-0.0015
2nd run	-0.0139	-0.0173	-0.0039
3rd run	-0.0145	-0.0182	-0.0043

Figure D. 2 Sublimation rate in SiO (44 µm D.) impregnated with Fe (3 wt% Fe); 1000°C - 5min

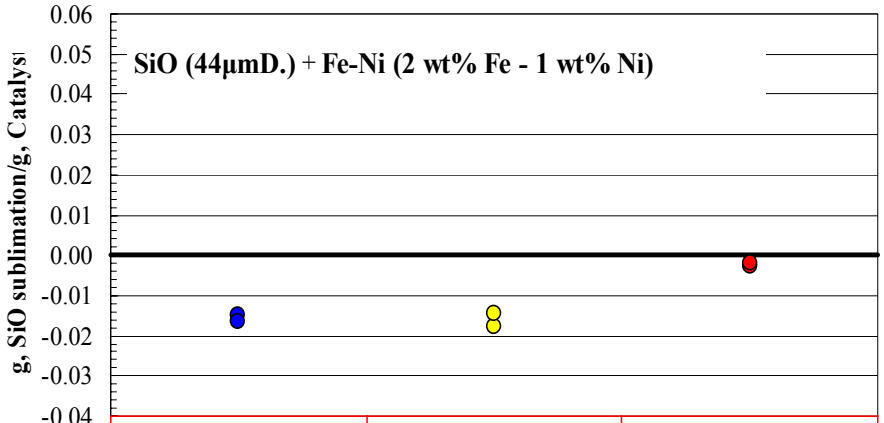

	NH3	N2	Ar
1st run	-0.0147	-0.0175	-0.0024
2nd run	-0.0268	-0.0145	-0.0027
3rd run	-0.0165	-0.0161	-0.0019

Figure D. 3 Sublimation rate in SiO (44 µm D.) impregnated with Fe - Ni bimetal (3 wt% Fe -1 wt% Ni); 1000°C - 5min

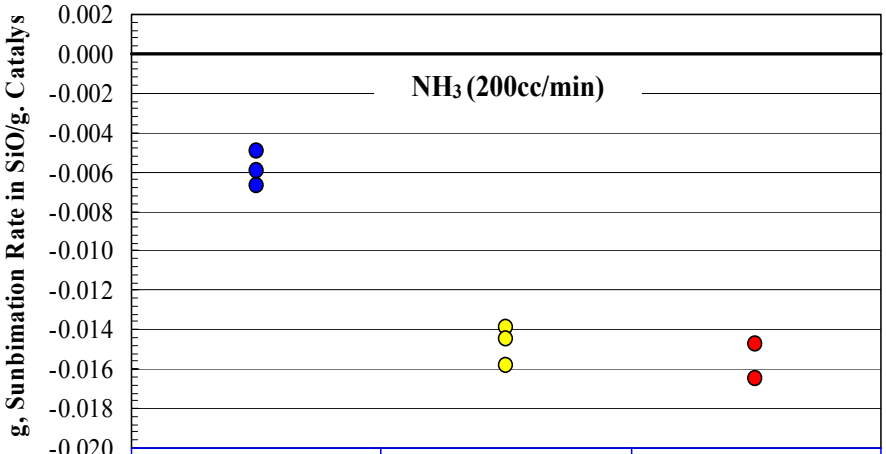

	SiO	SiO+Fe	SiO+Fe2/Nil
1st run	-0.00668	-0.01582	-0.01472
2nd run	-0.00496	-0.01387	-0.02683
3rd run	-0.00598	-0.01447	-0.01652

Figure D. 4 Sublimation rate (NH_3 feed rate = 200 cc/min); SiO, SiO + Fe (3 wt%), SiO + Fe-Ni (2 wt% Fe + 1 wt% Ni); 1000°C - 5min

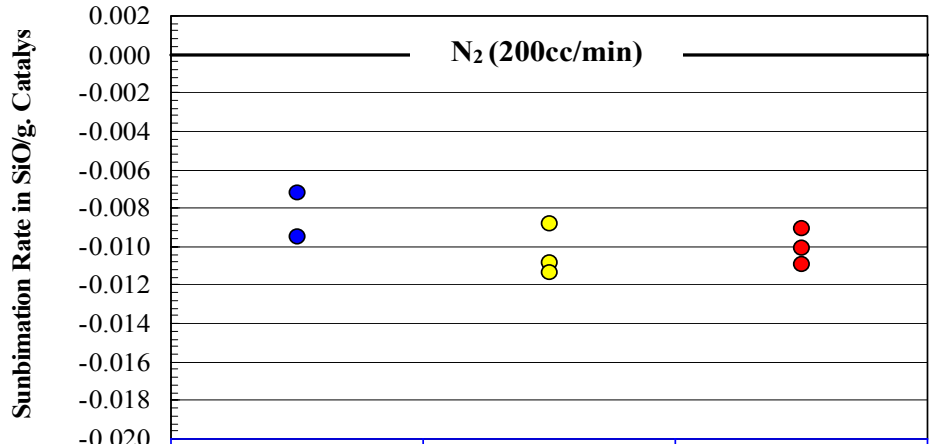

	SiO	SiO+Fe	SiO+Fe2/Ni1
1st run	-0.00952	-0.00880	-0.01097
2nd run	-0.00720	-0.01082	-0.00905
3rd run	-0.01812	-0.01135	-0.01007

Figure D. 5 Sublimation rate (N_2 feed rate = 200 cc/min);
SiO, SiO + Fe (3 wt%), SiO + Fe-Ni (2 wt% Fe + 1 wt% Ni); 1000°C - 5min

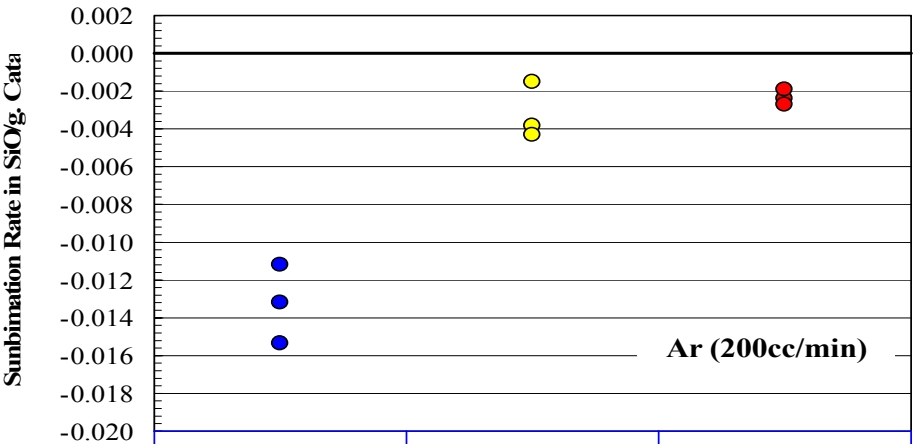

	SiO	SiO+Fe	SiO+Fe2/Ni1
1st run	-0.01319	-0.00154	-0.00239
2nd run	-0.01122	-0.00386	-0.00270
3rd run	-0.01540	-0.00434	-0.00191

Figure D. 6 Sublimation rate (Ar feed rate = 200 cc/min);
SiO, SiO + Fe (3 wt%), SiO + Fe-Ni (2 wt% Fe + 1 wt% Ni); 1000°C - 5min